Muon detection with scintillation detectors using indirect SiPM readout

von

Janina Struth

Bachelorarbeit in Physik

vorgelegt der

Fakultat fur Mathematik, Informatik und Naturwissenschaften

der Rheinisch-Westfalischen Technischen Hochschule Aachen

im September 2010

angefertigt im

III. Physikalischen Institut A

Prof. Dr. Thomas Hebbeker

Abstract

In the scope of this thesis prototypes of silicon photomultipliers with wavelength shifting fibres were measured for muon detection. This indirect readout happens with silizium photomultipliers (SiPM), which are coupled with the fibre.
The scintillator was wrapped with different reflective materials to optimise the light amplification. Furthermore two different thicknesses of the scintillator were used to have a comparison between the different light yield.
Consequentely different scintillator thicknesses were combinded and measured with different wrapping materials to compare their efficiency.

Zusammenfassung

In dieser Bachelorarbeit wurden Prototypen von Silikonszintillatoren mit einer wellenlangenschiebenden Faser zum Nachweis von Myonen vermessen. Diese indirekte Lichtauslese erfolgt mit Silizium Photomultipliern (SiMP), die mit der Faser verbunden sind. Der Szintillator wurde mit verschiedenen reflektierenden Materialien eingepackt um die Lichtverstarkung zu optimieren. Außerdem wurden zwei verschiednene Dicken des Szintillators verwendet um einen Vergleich zwischen der unterschiedlichen Lichtausbeute ziehen zu konnen.
Somit wurden verschiedene Szintillatordicken mit unterschiedlichen Materialien kompiniert und vermessen und anschließend auf ihre Effizienz hin verglichen.

Contents

1 Introduction

The LHC[1] is a circular particle accelerator with 27 km in circumference and in 175 m depth at CERN by Genf. In 2010 the LHC has four detectors: CMS, ATLAS, ALICE and LHCb.
The hige particle colliders search for new physics, e.g. new particles and provements for theoretical forecasts.
The Higgs boson is predicted to exist by the Standard Model in particle physics but is is not proven untill now. The physicists at CERN expect to prove the Higgs particle by detecting following events for example with muons:

$$H - \quad Z_0 Z_0 - \quad \mu^+\mu^-\mu^+\mu^- \tag{1}$$

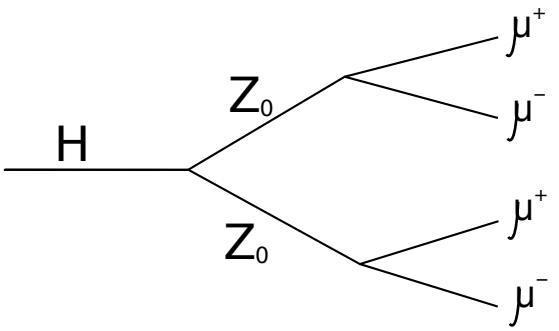

Figure 1.1: Feynman diagram of a possible Higgs decay

Probably in 2020 the LHC will be upgraded to SLHC[2]. At the moment the most probable upgrade is an increase of the peak luminosity up to 10^{35} $\mathrm{cm}^{-2}\mathrm{s}^{-1}$. By doing that much higher particle rates are reached inside the acceleration tunnel. To detect all araising events and to split one from the other the detectors need to detect and read-out very fast. The RWTH Aachen university collaborates at the CMS-Detector[3].
This thesis analyses the attributes of scintillation detectors using indirect SiPM readout to prove muons.
If this method seems to be auspicious it may will installed in the MTT[4] in CMS while the LHC is upgraded.

[1] Large Hadron Collider
[2] Super LHC
[3] Compact Muon Solenoid
[4] Muon Track fast Tag

2 Theoretical background

2.0 Cosmic muons

When cosmic ray particles enter the atmosphere they produce a cascade of lighter particles when they collide with molecules. The so called air shower is chematicaly shown in fig. 2.1.

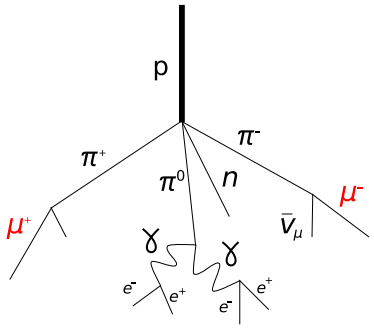

Figure 2.1: Typical air shower in the atmosphere where muons arise (adapted from [Wik07])

About 90% of the nuclear cosmic rays are protons, about 9% helium nuclei and 1% heavier nuclei. Cosmic ray has energies below about 10 GeV. In the collision of the nuclear ray with the particles in the atmosphere pions and kaons were produced. This unstable mesons decay into muons (especally the pions with a rate of 99,99%). Cosmic muons have a mean energy of about 4 GeV at the ground [GS07].
In this thesis the arising cosmic muons were used to charakterise a prototype of a muon detector.

2.1 Muon detection with scintillators

2.1.1 Scintillator

A scintillator is a material, that can be stimulated by traversing charged particles. The electrons in the molecules are raised to a higher energy level. A part of this excitation energy is released in form of optical photons while the molecules de-excite to their normal states (Fig. 2.2).

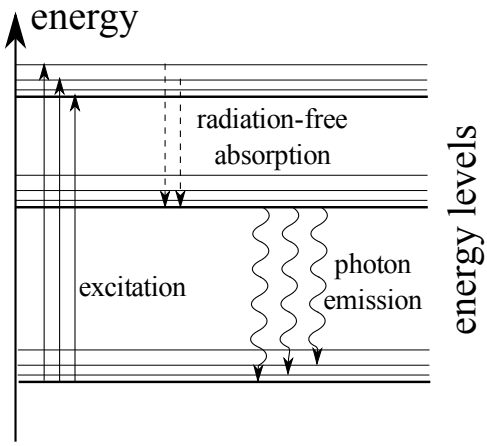

Figure 2.2: Schematic of the absorption and emission in a scintillator material

The amount of emitted light is dependent on the energy deposit. A photomultiplier measures the number of photons produced inside a scintillator. A scintillator can be made of organic or inorganic materials in liquid, gaseous or solid state.

2.1.1.1 Premium plastic scintillator BC-404

In the scope of this thesis the premium plastic scintillator BC-404 is used. This organic scintillator has the following advantages and disadvantages:

pro:	contra:
- fast emission	- not very radiation hard
- flexible detector design	- poor energy resolution
- simple production, comparably unexpensive	
- good time resolution	
- good light yield	

To raise the efficiency of the scintillator it is wrapped into a reflective foil. Simulations have shown that an air gap between the scintillator surface and the wrapping material is more efficient than a direct coating [Pap10]. In the scope of this thesis different foil materials will be examinated.

2.1.2 Wavelength shifting fibre and optical cement

Wavelength shifting (WLS) fibres are used to extract photons from the scintillator to which the WLS fibre is coupled optically in a groove by an optical cement.
The optical cement needs to have a similar refraction index as the scintillator material so that the photons can be transmitted to the fibre without reflecting. The optical cement BC-600 fulfils this qualification. It has a refraction index $n_{opC} = 1.57$ and a density of 1.18 gcm^{-3} [Tec07].
The WLS fibre absorbs photons and re-emits them with higher wavelenghts so that self-absorption of the fluorescence medium is disabled.

The fibre in the scope of this thesis has a polysterene core with a refraction index $n_{core} = 1.60$. The inner cladding is made of polymethylmethacrylate with $n_{inner} = 1.49$ and the outer cladding is made of fluorinated polymer with $n_{outer} = 1.43$ [SG05].
Figure 2.3 shows a typical photon trajectory in a WLS fibre with round cross section.

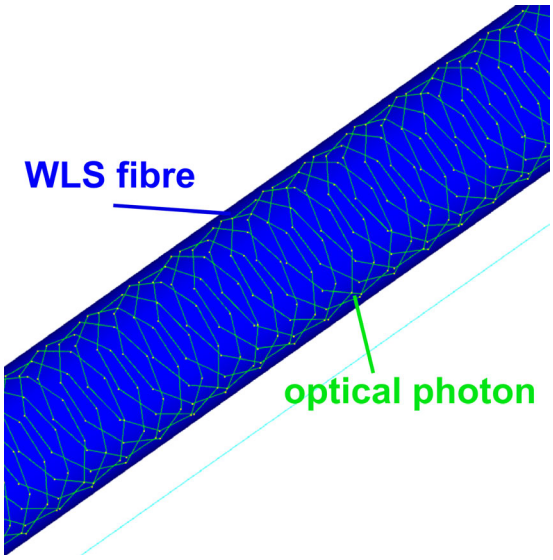

Figure 2.3: Sketch of an optical photon trajectory in a circular mode inside a WLS fibre [Pap10].

2.1.3 SiPM

For the muon detection with a scintillation detector a silicon photomultiplier (SiPM) is used. It is a multipixel semiconductor photodiode, where each pixel is an Avalanche photodiode (APD). The pixels are joint together on a common silicon substrate where the signal can be tapped at aluminium strips (see fig. 2.4) [EHG01].

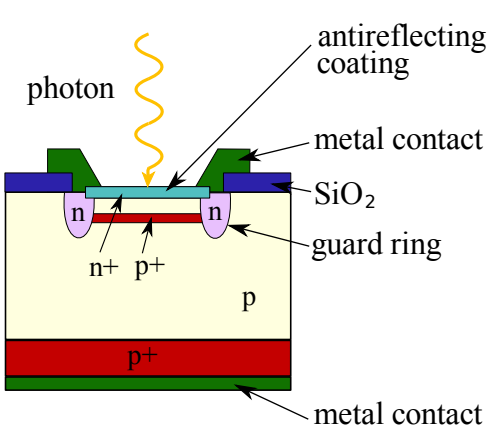

(a) Schematic construction of an APD (adapted from [Bar04])

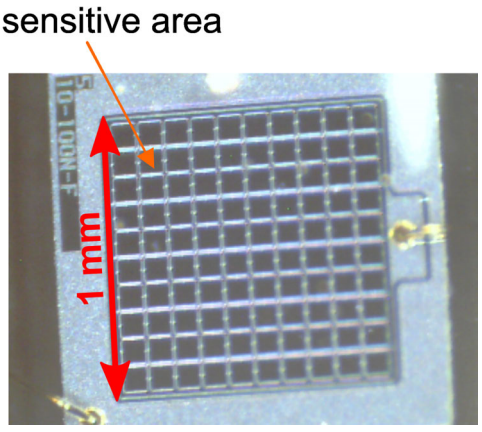

(b) Photo of a SiPM [Mer10]

Figure 2.4: APD schema and SiPM photo.

The output signal is a sum of the signals from all pixels fired, because all SiPM pixels work together on common load (see fig. 2.5).

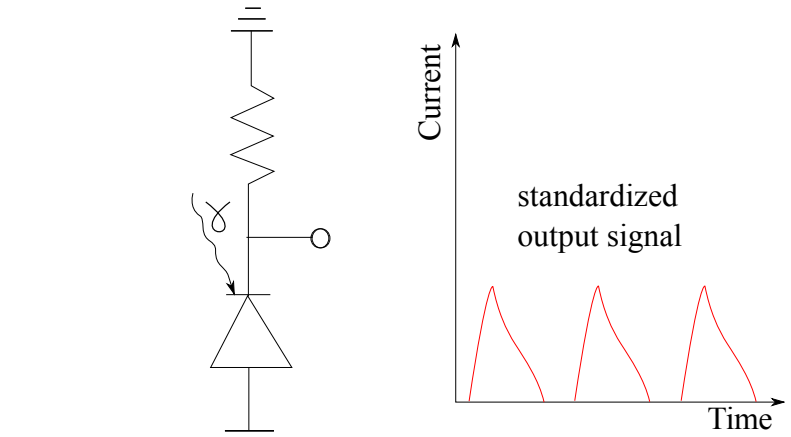

(a) APD

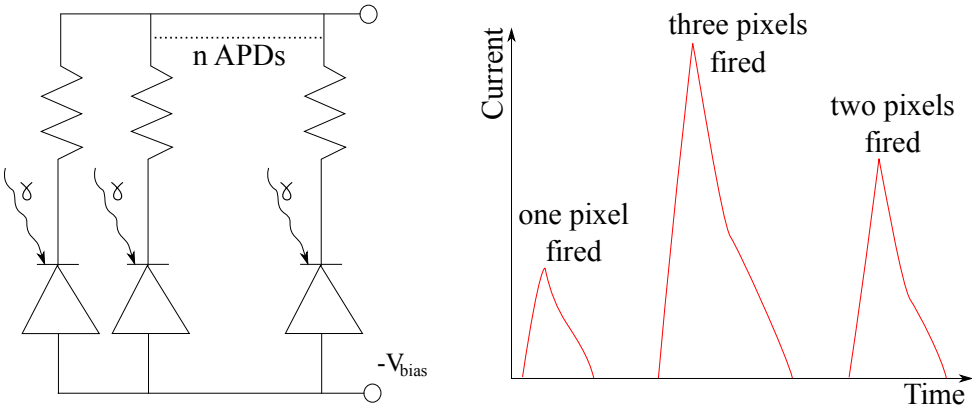

(b) SiPM

Figure 2.5: Signal output of an APD and a SiPM (adapted form [Din06]).

Not the whole area of the SiPM is sensitive, because many APDs were joint together there is some space between them where other electronic devices were placed. The fill factor ϵ gives the percentage of the sensitive area in comparison to the whole area. The photon detection efficiency η_{eff} is given by

$$\eta_{eff} = \eta_q \cdot \epsilon \cdot P_{trigger} \tag{2}$$

with the quantum efficiency η_q and the probability that an incoming photon causes a signal P_{signal} [RL09].

Table 1: Key specifications of the S10362-11-100C SiPM

effective area	1×1 mm
number of pixels	100
pixel size	100×100 μm^2
fill factor ϵ	78.5%

2.1.4 Wrapping materials

As noted in chap. 2.1.1.1 a reflective material wrapped around the scintillator raises its efficiency.
In this experiment different wrapping materials e.g. TYVEK 1073B and common aluminium foil are used to examin their influence on the scintillator efficiency.
TYVEK is a synthetic material with thermally welded high-density polyethylene fibers. It is approximately 90% reflective in the visible, dropping by a few percent as the angle of incidence increases [Gic98] which fits to the spectrum of the BC-404 scintillator.
Fig. 2.6(a) shows the photon emission spectrum of scintillator BC-404 where the peak is at roughly 410 nm in the visible.
The maximum of the photon detection efficiency of the used S10362-11-100C SiPM (fig. 2.6(b)) fits well to this emission spectrum, what is very important for a precise muon detection.

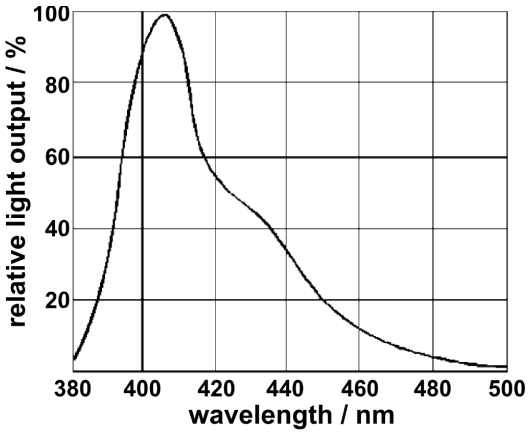

(a) Photon emission spectrum of scintillator BC-404 as given by the manufacturer [CI05].

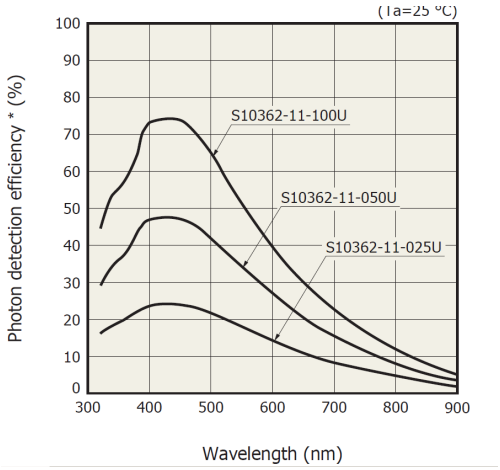

(b) Photon detection efficiencies for 1×1 mm SiPMs at 25°C [K.K10].

Figure 2.6: Wavelength dependency of the SiPMs and the BC-404 scintillator

The results are compared to a measurement without a wrapping material when the photons are only reflected due to total internal reflection. To realise this the scintillator is wrapped into black felt because the setup has a lot of metal where the photons could be reflected what would falsify the measurement. Table 2 lists the reflectivities of the different wrapping materials.

Table 2:

wrapping material	reflectivity
TYVEK	90% [Gic98]
aluminium foil	88% [Han05]
black felt	∼0%

2.2 Signal processing

2.2.1 Amplifier boards

The SiPMs are connected to amplifier boards where the supply voltage U_{sup} for the SiPM is set. The supply voltage of typically 75 V can be adjusted to the given operation voltage (72.5 V) of the SiPM with help of a voltage stabiliser mounted on the board.

The voltage set can be measured at a point of control and at the SiPMs themselves. As shown in fig. 2.7 the voltage set (lower than 72,5 V) is a little higher than the real voltage at the SiPM and at the point of control.
Over the supply voltage of 72,5 V is a constant connectedness. That is because of the adjustment of the potentiometer. This plot shows, that a lower voltage at the SiPMs could set from outside by changing the supply voltage but not a higher voltage. For that the potentiometer need to shift.

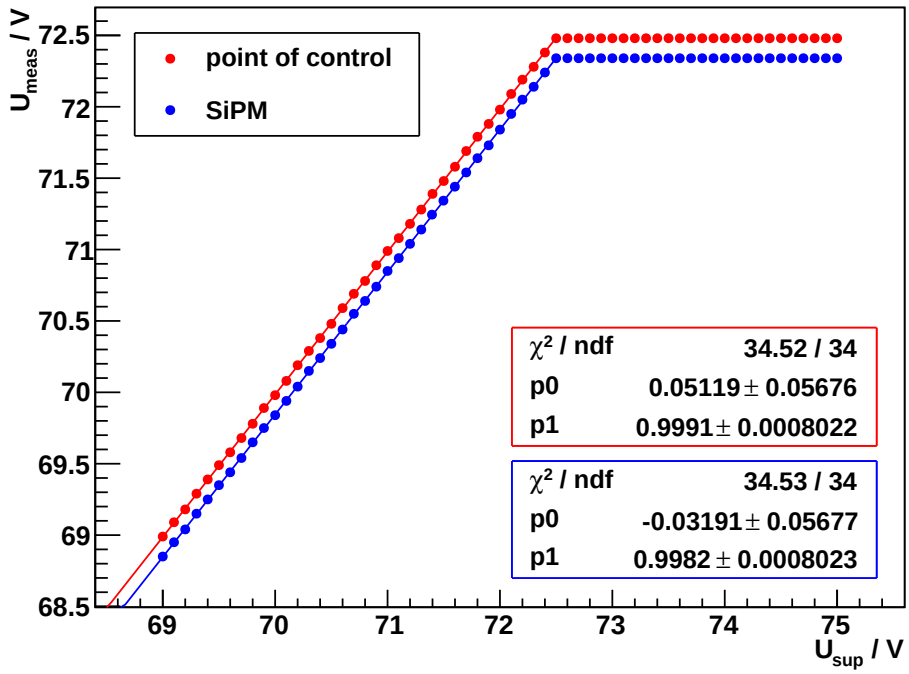

Figure 2.7: Voltage connectedness with fit function $p1 \cdot U_{sup} + p0 = U_{meas}$

The plot in fig. 2.7 shows that the real voltage at the SiPMs is lower than the invested voltage, but the difference is nearly linear.

2.2.2 Discriminator

2.2.3 Charge to digital converter (QDC)

A charge to digital converter (QDC) measures the charge of an event by integrating the incoming voltage signal.

2.2.3.1 Model V965 CAEN

The incoming signal is converted parallel into two signals that have a different range and accuracy. The high channel has a range of $0 \div 900$ pC with 200 fC/count and the low channel has a range of $0 \div 100$ pC with 25 fC/count [CAE08].
The QDC pedestal is the value readout that is measured when no input signal is present while the input is open. It is mainly due to a basic current that is needed for a proper working of the QDC and which is also integrated. The pedestal peak marks the zero point.
The QDC has 4096 channels ranging from 0 to 4095 what corresponds to 81.92 nC. The last 255 channels (from 3840 on) are filled with the overflow. The overflow has this width because of the sliding scale that optimises the resolution of the data by adding a random equivalent of 0 to 255 channels to the signal. After processing of this signal the overflow (signal higher than the range) is filled in the last channel minus the random channel.
Figure 2.8 shows a typical QDC spectrum.

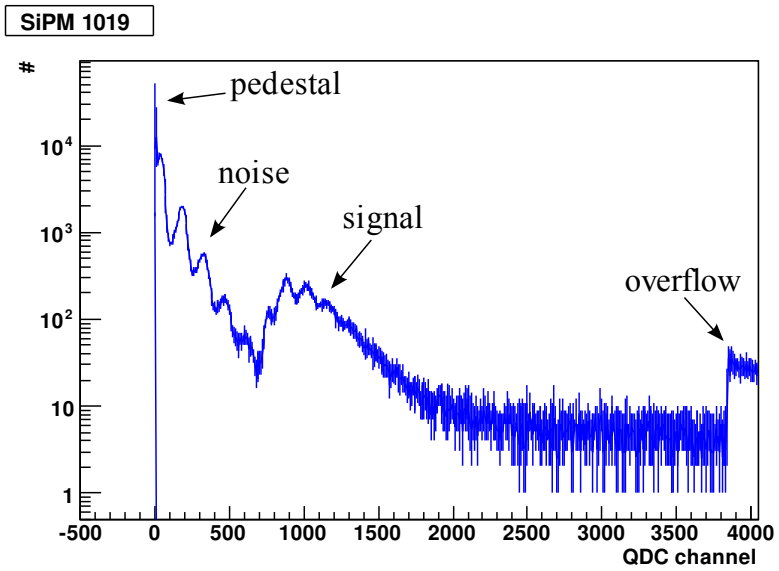

Figure 2.8: QDC spectrum

2.2.4 Temperature sensors

To control the temperature during the measurement the temperature sensors on each bord and 19 seperate sensors inside the dark box were read out.
The sensors are of the type DS18B20 by Maxim. Every sensor has an unique ID so that the sensors near the SiPMs were processed seperately and the temperature output of other ones is averaged.
The sensors have an operating temperature range of $-10°C$ to $+85°C$ with an accurate to $\pm 0.5°C$ and a maximum read out time of 750 ms [Pro08].

3 Setup

3.1 Scintillator

The dimensions of the scintillators regardet in the scope of this thesisare $100 \times 100 \times 8$ mm^3 and $100 \times 100 \times 6$ mm^3. In the middle is a groove where the wavelength shifting fibre is inserted and coupled by an optical cement to the scintillator. The SiPMs are movably connected with the ends of the fibre coupled by an optical gel (see fig. 3.1).
The scintillator is wrapped into a reflective material so that the photons can t leave the scintillator. They are reflected into the wavelength shifting fibre, which conducts them to the detectors.

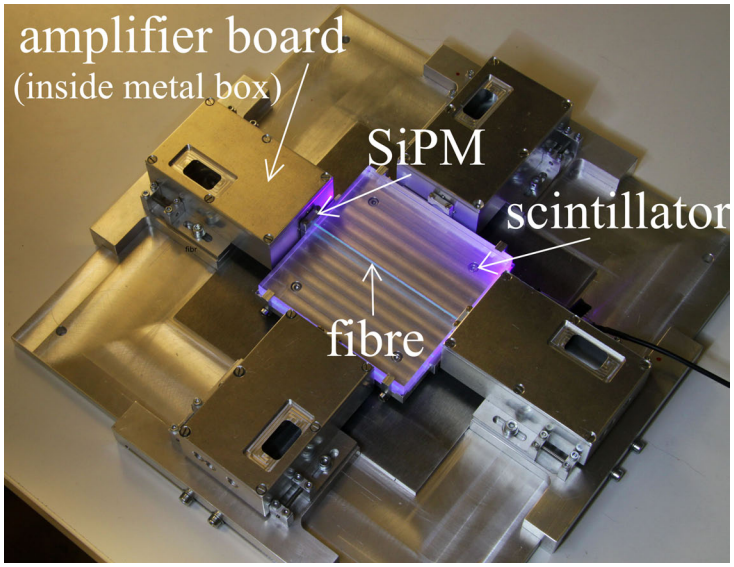

Figure 3.1: Scintillator setup with fibre and positions of the SiPMs with the amplifier boards (adapted from [Heb10]).

3.2 SiPMs and amplifier boards

Each SiPM is connected to an amplifier board where the oparation voltage U_{op} (c.f. tab. 3) is adjusted.

Table 3: Manufacturer data of the SiPMs:
HAMAMATSU MPPC at 25°C (p.e.=photon equivalent)

	1018 SiPM	1019 SiPM
Type No.:	S10362-11-100C	S10362-11-100C
Serial No.:	1018	1019
U_{op}	71.29 V	71.29 V
Darkcount rate / s	680K (0.5 p.e. thr)	735K (0.5 p.e. thr)

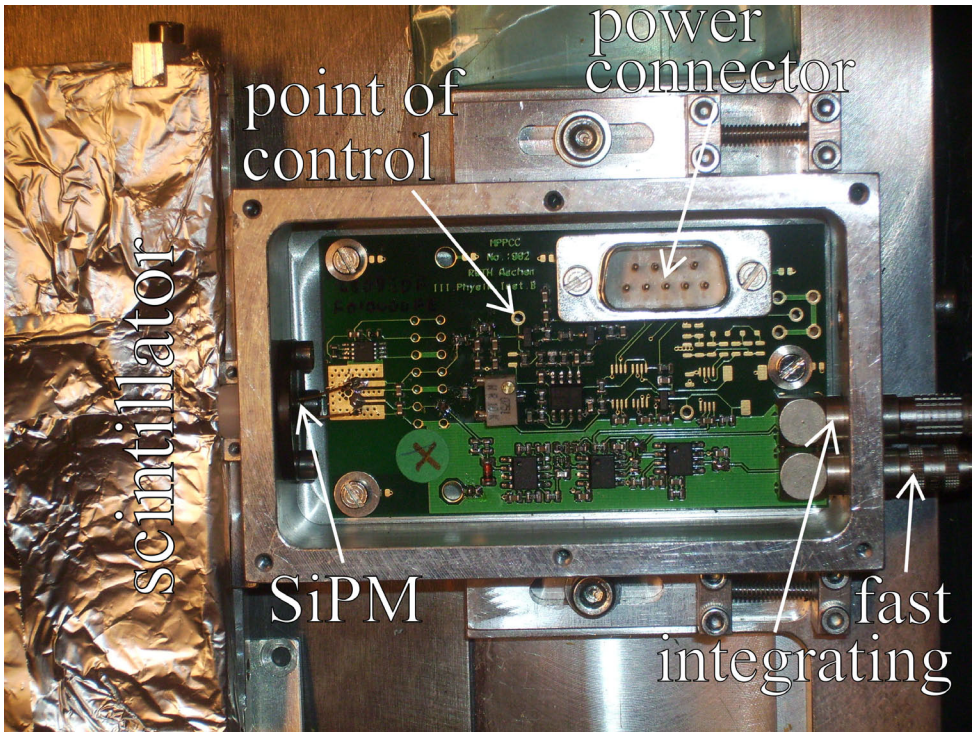

Figure 3.2: Photo of the amplifier boards with the soldered SiPM and connected with the fibre.

The two output signals, fast and integrating channel, shown in fig. 3.2 are processed seperately (c.f. chap. 3.5).

3.3 Hodoscope

The whole experimental setup is situated in a dark box to shield it from other photons than the ones that are generated by traversing muons inside the scintillator.
The dark box is mounted between two scintillator tiles that are read out by the photo-multipliertubes. These PMTs act as a trigger for cosmic muons. The distance between the PMs limits the solid angle and with it the number of detectable muons.

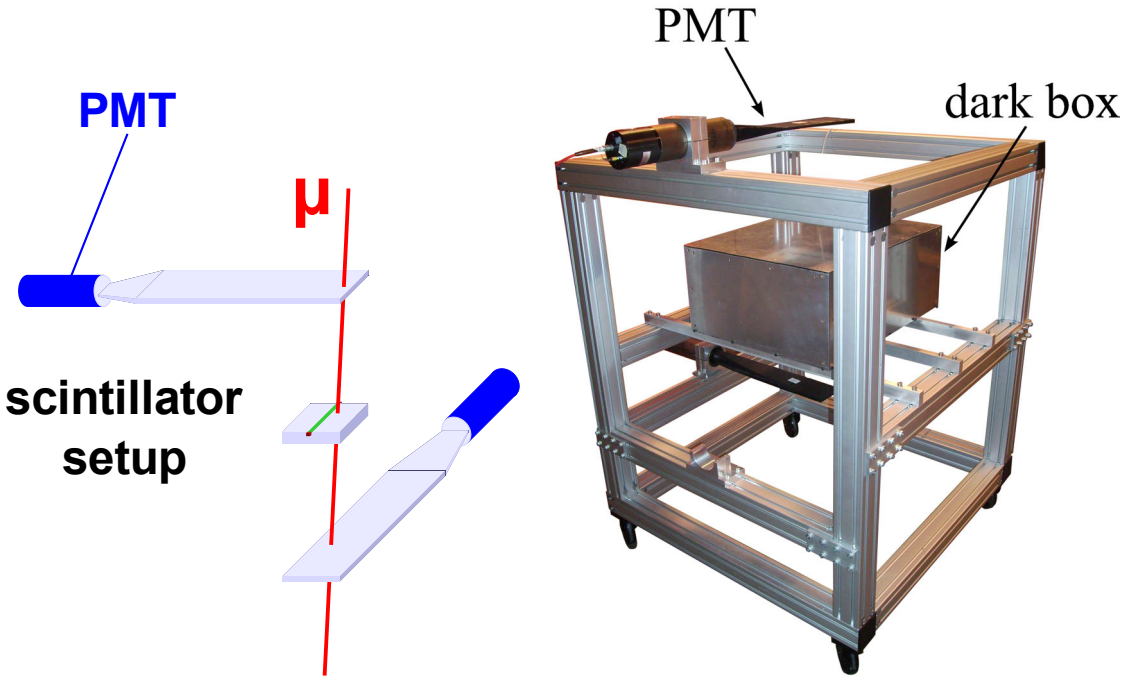

(a) Schematic view of the hodoscope setup without the dark box (adapted from [Pap10]).

(b) Photo of the hodoscope.

Figure 3.3: Hodoscope

3.4 Working principle

A muon that passes the scintillator releases optical photons (chap. 2.1.1). These photons are reflected at the polished surface of the scintillator and at the wrapping material respectively. When they pass the wavelength shifting fibre (chap 2.1.2) they are absorbed and re-emited with a higher wavelenght. These photons run through the fibre to the sensitive area of the SiPMs (cf. fig 3.4).

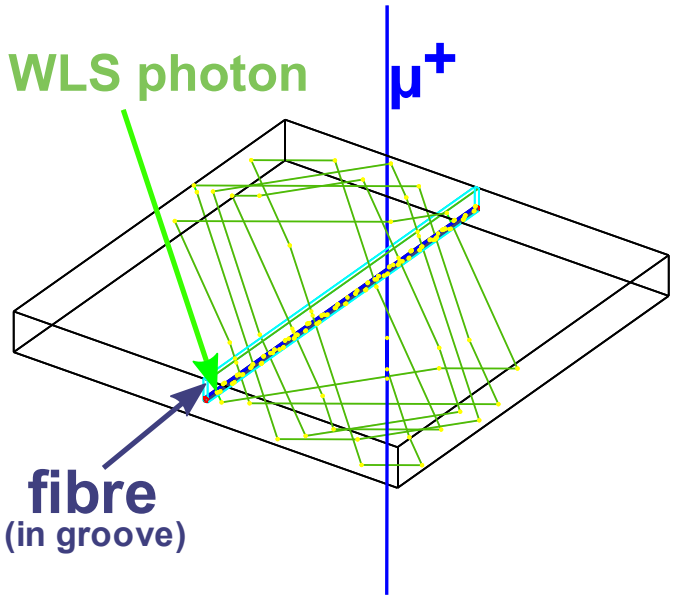

Figure 3.4: Working principle of the scintillator with WLS fibre [Pap10]

3.5 Circuit diagram

The two SiPM signals, fast and integrating channel, are processed seperately.
The fast channel signal runs through the discriminator where the threshold (c.f. chap. 4.1.1) is adjusted. The SiPMs have a threshold of about 140 mV and the PMTs about 300 mV. Both have an output signal lenght of about 50 ns.
After the discriminator the SiPM signals need to be delayed, so that they fit to the PMT signals. All these signals come together in an "OR". There the output signal triggers everytime when at least one single signal comes in. A counter counts the number of trigger events.
The trigger signal and all single signals then are processed in the QDC and after that read out by a computer.

The integrating channel signal is processed directly in the QDC, while a trigger signal (coming from the "OR") was given, and then read out by the computer, too.
Figures 3.6 and 3.5 show the circuit.

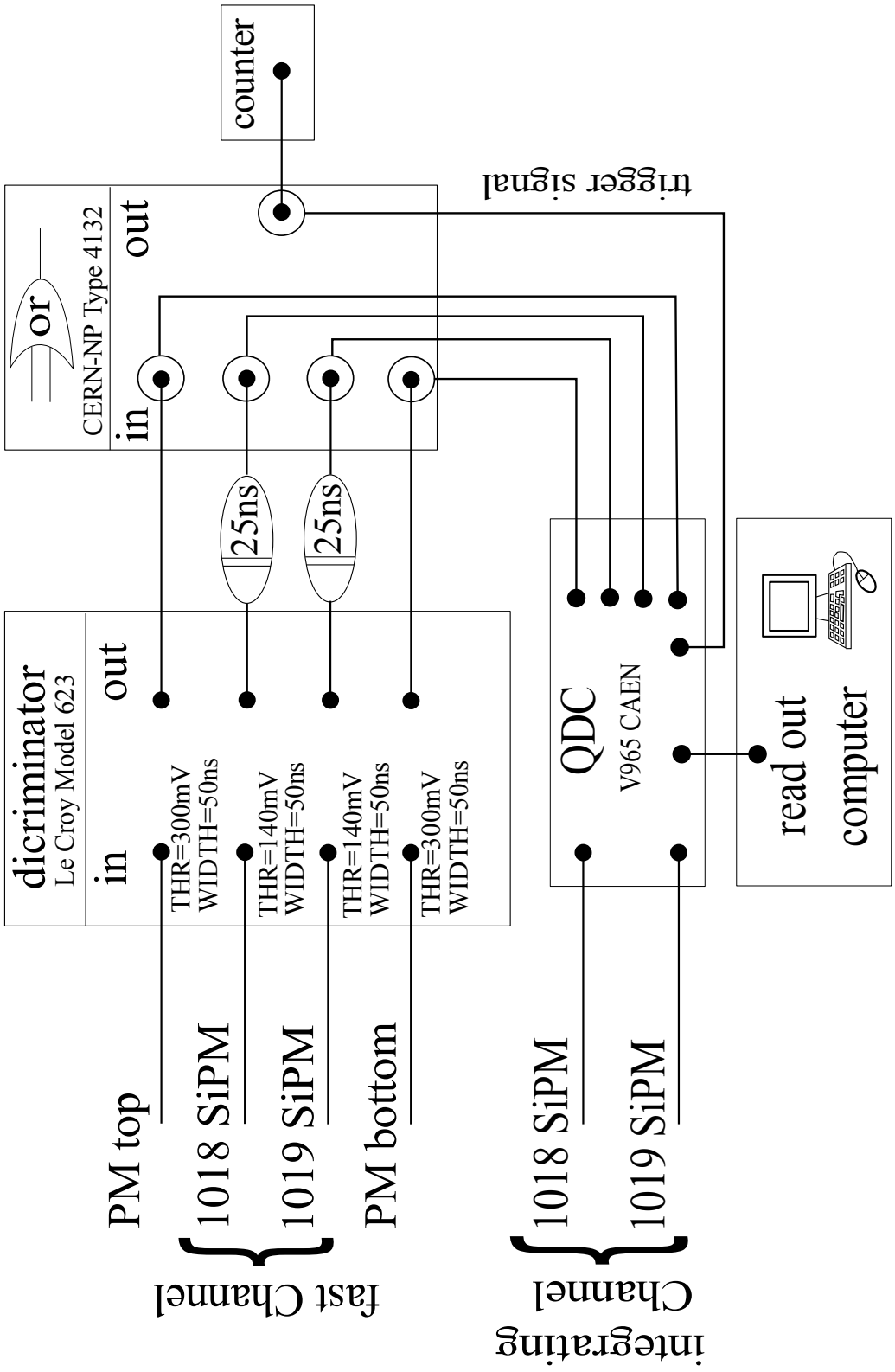

Figure 3.5: Schematic circuit diagram of the signal processing

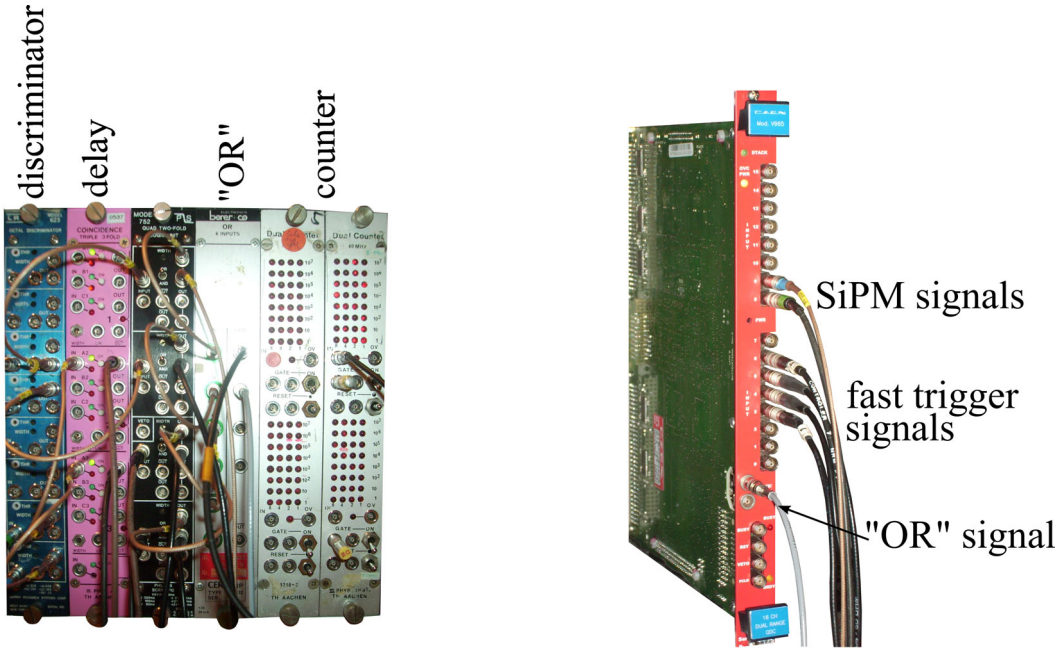

(a) Discriminator, delay (coincidence), OR and the counter. (b) QDC modul

Figure 3.6: Photo of the circuit of the signal processing.

With such a circuit every singnal is read out seperately and different signal combinations can be examine. For example the QDC spectrum could plot if both SiPMs have a signal of if just one triggers. Combinations with the PMT also is possible.

The width of the discriminator signal is ascertained with the help of the oszilloscope. The width needs to match to the signal width (c.f. fig. 3.7).

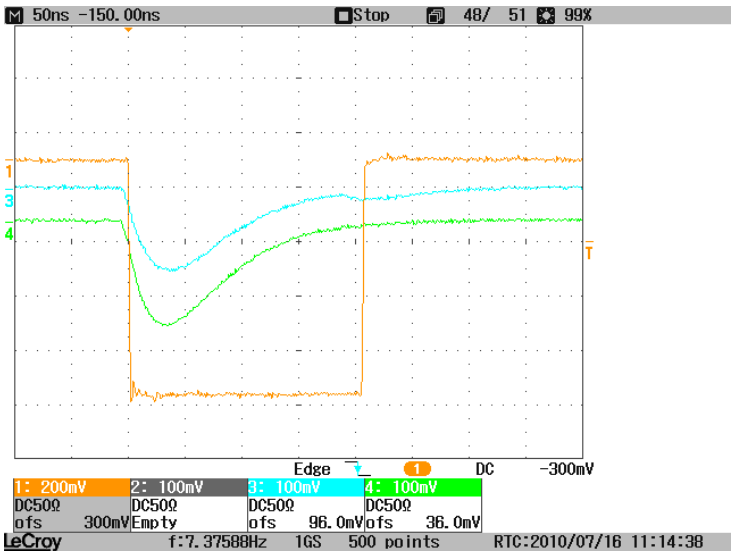

Figure 3.7: Ascertainment of the width of the discriminator with the help of the hodoscope orange=discriminator width; cyan,green= SiPM signals

4 Measurements

4.1 Devices characterisation

4.1.1 SiPM noise

The characteristics of the noise pulses of the SiPMs are exemplarily shown in fig. 4.1 RECORDED with the oscilloscope.

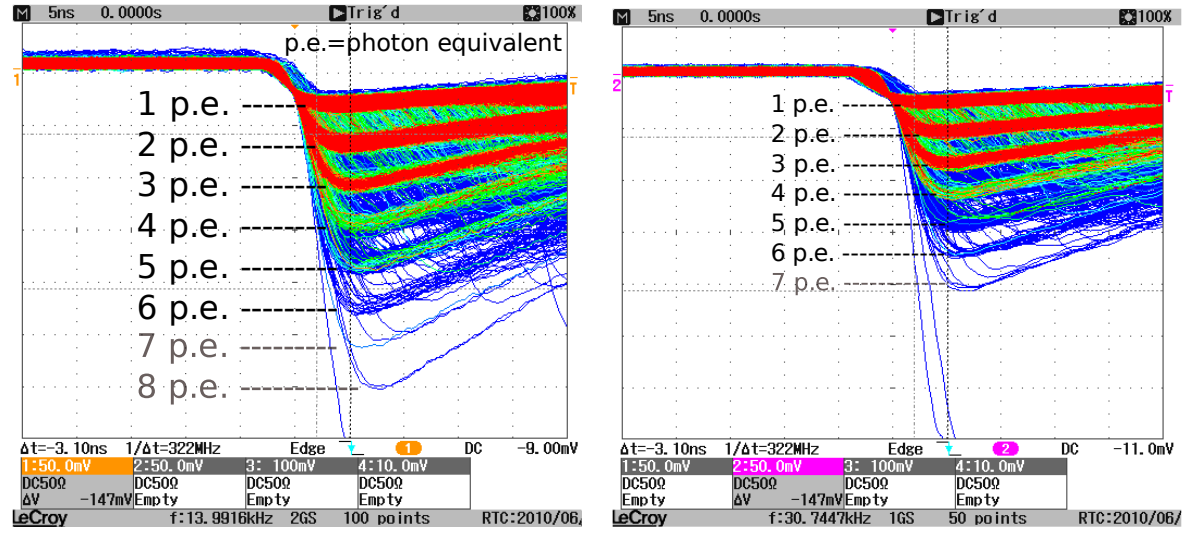

(a) 1018 SiPM:
One photon amplitude corresponds to roughly 44 mV.

(b) 1019 SiPM:
One photon amplitude corresponds to roughly 38 mV.

Figure 4.1: SiPM noise measured with the oscilloscope.

These oscilloscope charts illustrate the photon equivalent pulses of the noise only. The lowest pulse amplitude is the equivalent to one photon pulse and higher pulses have amplitudes that are a multiple of that. The amplitude of one photon equivalent is averaged over the different pulses.
Figure 4.1 shows the collection of SiPM pulses at different times. The colour red identifies recent and the colour blue older events.

The threshold at which the trigger is adjusted can be calculated by the mean of one photon equivalent. Then the noise rate is measured while the trigger is adjusted between two photon equivalents so that the lower one is no more measured but the higher one completely.
As a result of the uncertainty of measurement, because of the width of the signals, the trigger is varied about two accuracy steps of this adjustment. The half of the width of this interval of the noise rate corresponds to the uncertainty of the measurement.
As shown in fig. 4.2 the noise rate and the threshold have an exponential dependency (Data see appendix tab. {10}).

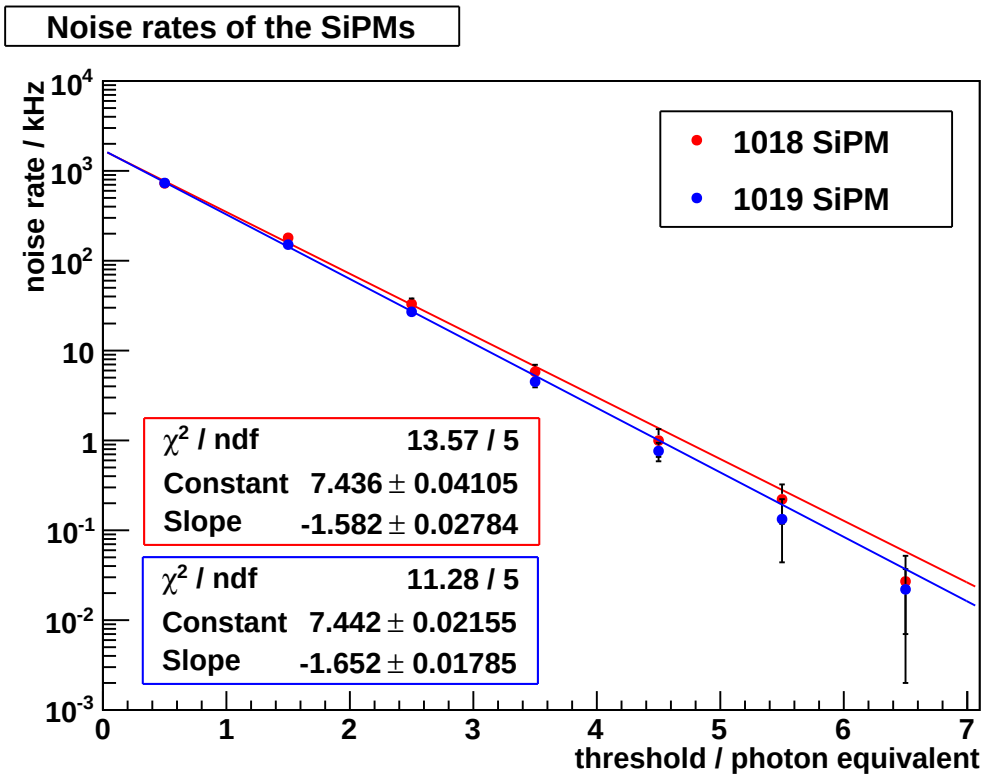

Figure 4.2: Diagram of the noise of the SiPMs with logarithmic ordinate

At a threshold of four photon equivalents the noise rate is insignificantly small so that the threshold for the measurement of cosmic muons is adjusted at ∼140 mV.

4.1.2 Temperature

The measurements run about 5 or 6 days to collect enough events to have significant statistics. During that time the temperature changes between day and night up to 5°C, but the operation voltage U_{op} (cf. tab. 3) refers to 25°C.
Figure 4.3 shows the chronological development of the QDC spectrum (a) and the corresponding development of temperature (b).
As can be seen, because of the same time axis, the diagrams are correlated and let suppose that lower temperatures means better QDC spectra. The measurements in the time intervals form 0 to 20 and from 100 to 140 are at low temperatures and have the clearest spectra, but in the measurement at a very high temperature (from 60 to 80) no p.e. signal peaks can be seen plainly. The data lower than 500 channels are a result of the noise. This plot has a cut on the trigger channel, when the trigger signal is greater than 2000 channels to cut the noise. At low temperatures the noise is more pronounced and sometimes higher than the cut.

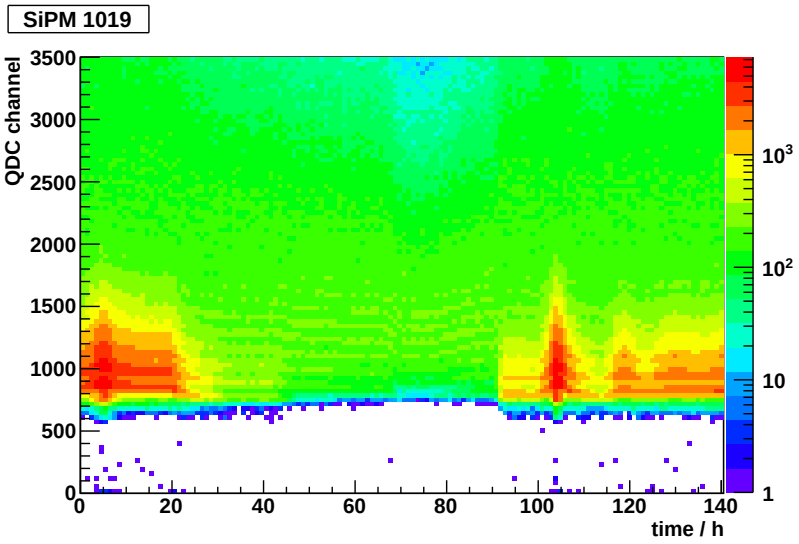

(a) Chronological developement of the QDC spectrum.

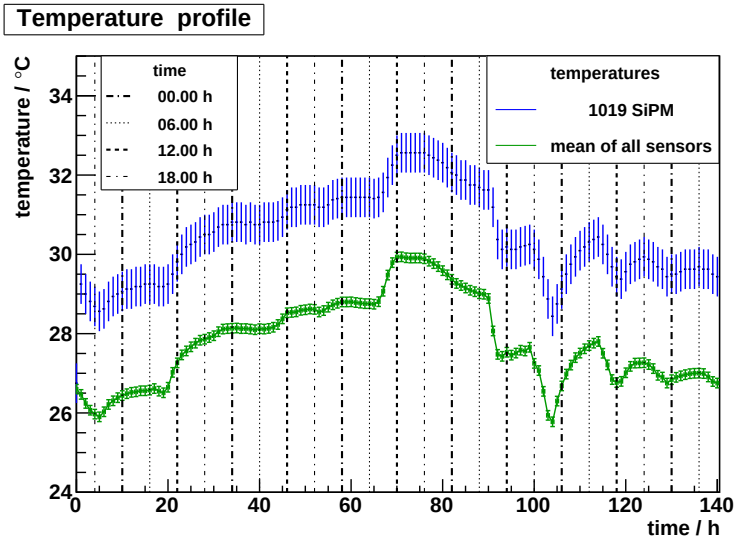

(b) Chronological developement of the temperature in the setup.

Figure 4.3: Time and temperature dependency of the QDC spectrum.

The dependency on the reverse voltage on the temperature has been studied in [Ren10]. The characteristic curve slides with lower temperature to lower voltages (see fig. 4.4).

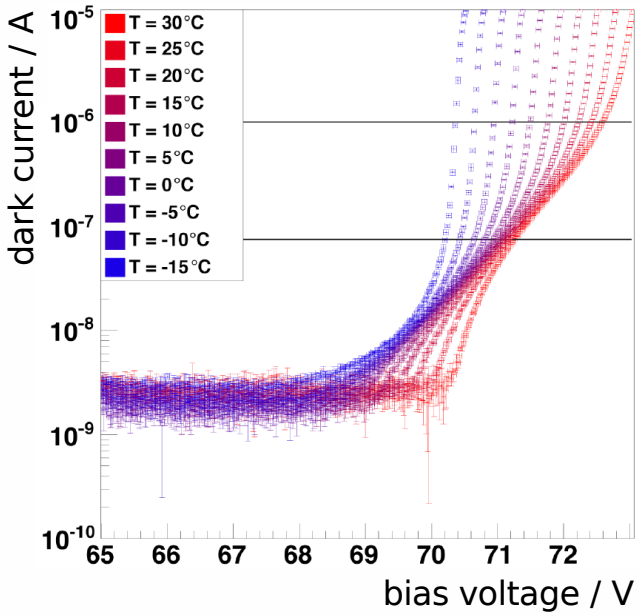

Figure 4.4: Characteristic curve of a Hammamatsu SiPM Typ-50C1 with 50 μm × 50 μm pixels [Ren10].

The operation voltage is adjusted at a fixed point given by the manufacturer but at 25°C. Normaly the voltage need to be changed about 56 mV per °C [K.K10].
This is the reason why the QDC spectrum is dependent on the temperature, because with different temperatures the operation voltage U_{op} moves to different values.

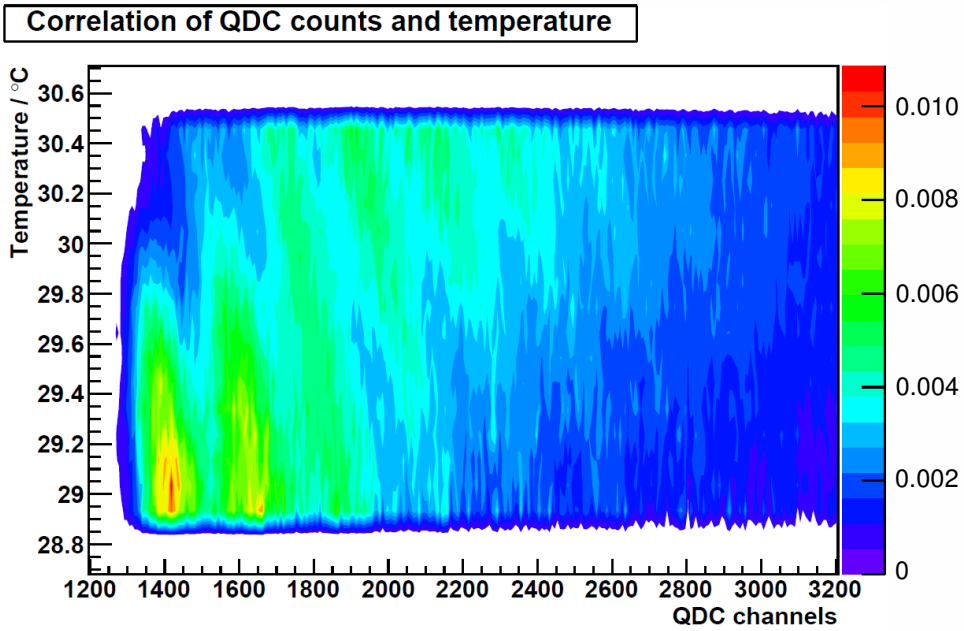

Figure 4.5: Temperature dependency of the QDC spectrum.

Fig. 4.5 shows the QDC spectra in dependency on the temperature normalised to the

same number of events. It can be seen, as described before, that the spectrum changes with different temperatures.
The QDC counts of the peak position change in dependency on temperature. ΔQDC_i means the middled difference in QDC counts of peak i by a temperature variation of ΔT (see tab. 4).

Table 4: Variation of the peak position with $\Delta T = 0.5°C$

i	ΔQDC_i
1	45±10 QDC counts
2	50±10 QDC counts
3	45±10 QDC counts
4	45±10 QDC counts
5	50±10 QDC counts
6	50±10 QDC counts

Therefore a temperature difference of 0.5°C means a QDC count difference of about (45 to 50)±10 QDC counts.
As a result of that the spectra will be evaluated at same temperature intervals to have comparable data.

4.2 Muon measurement

In the following different signal combinations were examine in the different measurements and wrapping materials. Veto means no signals higher than the noise (threshold of 2000 channels) and SiMP 1019, SiPM 1018 and PMT means signals higher than the noise of these PMs.
As described before the QDC pedestal peak marks the zero point (chap. 2.2.3). To shift the spectra every pedestal is determined by a gaussian fit (see fig. 4.6). After that its value is substrated to every corresponding data. For that only the pedestal position is of interest but not the high.

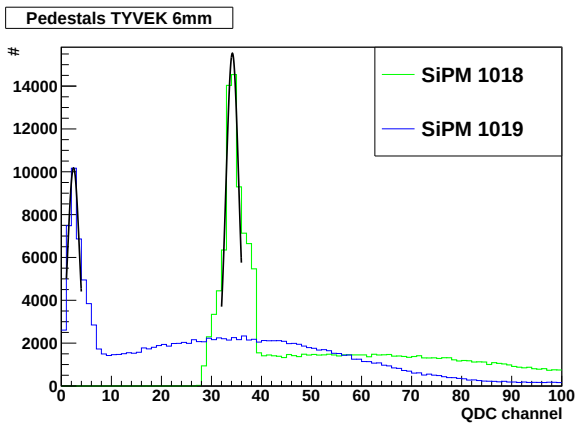

Figure 4.6: Gaussian fit to the QDC pedestals exemplarily with TYVEK 6 mm.

The temperature varied between 25°C and 32°C during the measurement. As described in chap. 4.1.2 the data should be evaluated at same temperature intervals, but the measurements with black felt have no data in the temperature interval of the other measurements (see tab. 5). The interval range is about 0.5°C respectively 0.6°C to have comparable data with significant statistics. The two scintillator thicknesses are evaluated at same temperature intervals.

Table 5: Temperature intervals of the measuerements

wrapping material	temperature interval / °C
black felt	29.8 - 30.3
TYVEK	26.6 - 27.2
aluminium foil	26.6 - 27.2

4.2.1 Black felt

4.2.1.1 Scintillator 8 mm

The trigger rates of the SiPMs varied during the measurement (fig. 4.7(a)). This is because of the changing of temperature. The rates curve is qualitatively the inverse of the temperature profile. Low temperatures means high rates and high temperatures means low rates.
The rate of the PMT shows no temperature dependency and has a constant rate of 4.71 s^{-1}.

As can be seen in fig. 4.7 SiPM 1019 has a lower rate than SiPM 1018. That implies that SiPM 1019 had a higher threshold and with that less noise than SiPM 1018. This can also be seen in fig. 4.8: The red curve (SiPM 1018) in (a) has a higher noise amount than the green curve (SiPM 1019) in (b). These curves corresponds to the signals which one SiPM saw if the other had a signal higher than the treshold. SiPM 1019 has more noise than SiPM 1018 what represents the lower trigger rate, too.
It is also impossible that the wavelenght shifting fibre was coupled to the SiPMs with different accuracy and had a better transition to SiPM 1018.

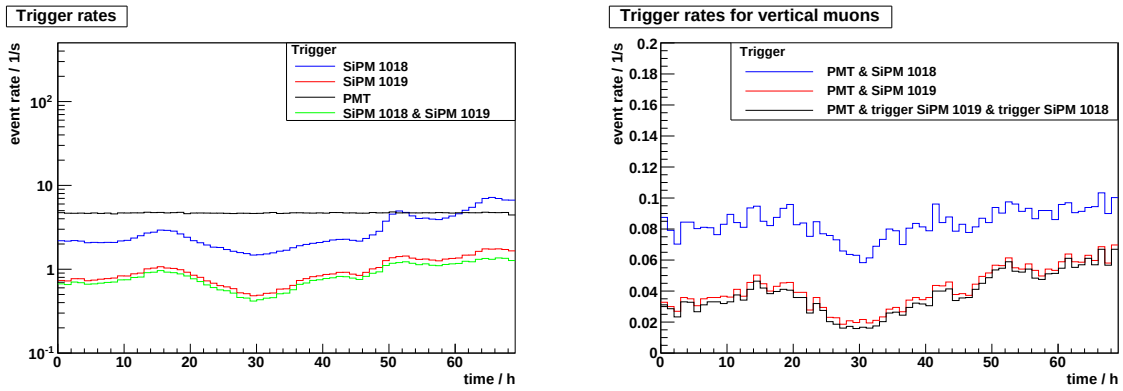

(a) Rates of single detectors with logarithmic ordinate

(b) Rates of vertical muons

Figure 4.7: Trigger rates of the measurement with black felt 8 mm.

The trigger rates for vertical muons are dependent on the temperature. The PMT has no temperature dependency (fig. 4.7(a)) but the single detector rates for the SiPMs are much lower than the ones of the PMT and as a result from that the rates for vertical muons show a dependency on temperature, too.

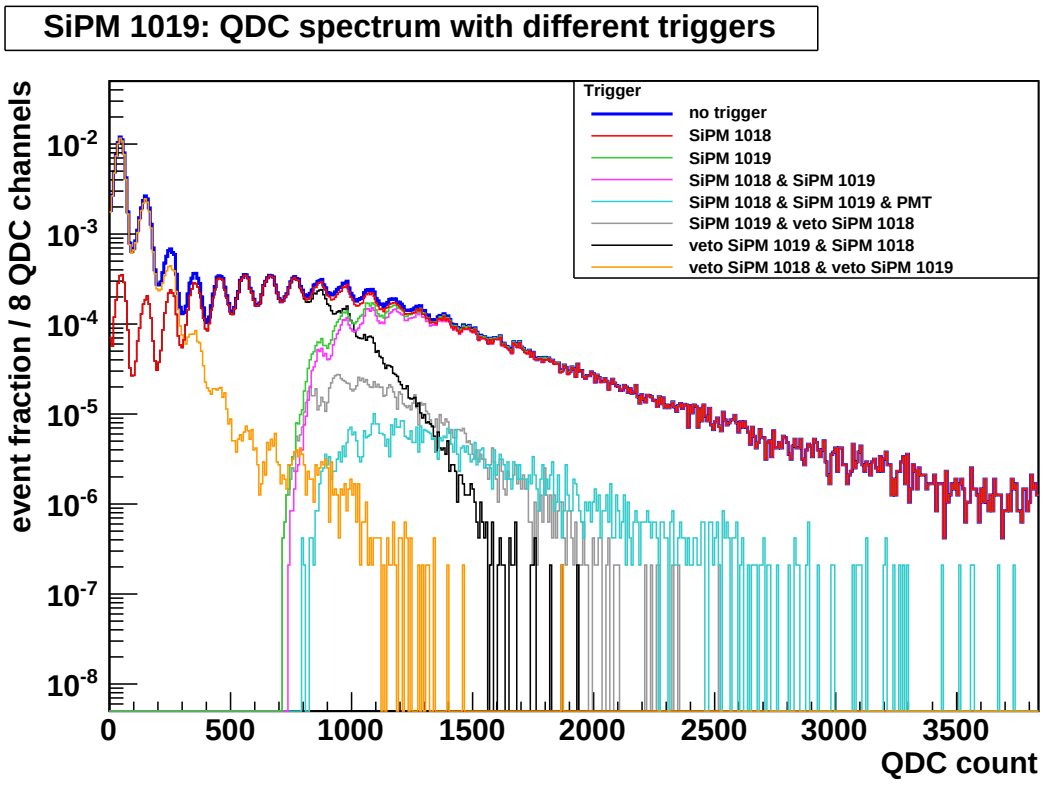

(a) QDC spectrum of channel 9

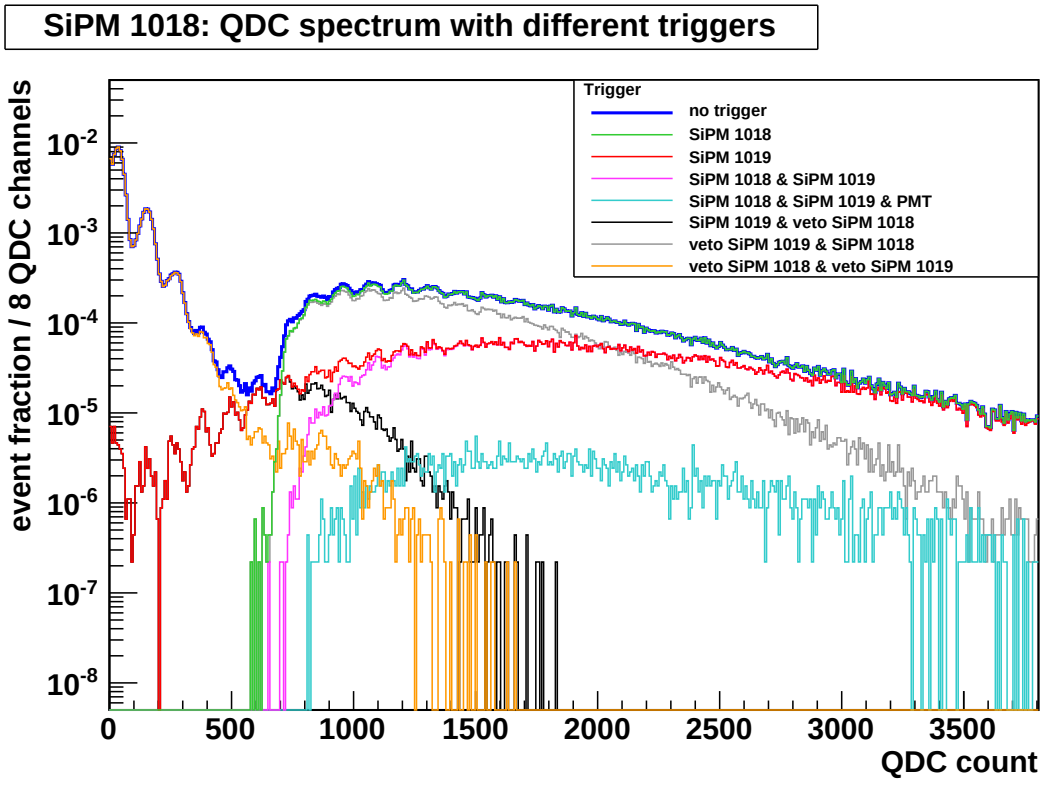

(b) QDC spectrum of channel 8

Figure 4.8: QDC spetra with different triggers of the measurement with black felt 8 mm.

The QDC spectra in fig. 4.8 are normed to the blue curve (no trigger) to have comparable data to the other measurements. For that the integral ober the blue curve is set to one, because this curve contains all signals.
The orange curve (veto SiPM 1018 & veto SiPM 1019) should not correlate with the green curve (SiPM 1019) in (a) and (SiPM 1018) in (b), because the orange one should have only noise and the green one only signal. The overlap of the curves could be a result of the gate width of 200 ns. A typical signal on average is 100 ns witdh. To ensure that all signal is in the gate, this bigger width was used. But then it could happen, that two low noise signals are in one gate. Alone they would not top the threshold to be signals, but together they are high enought to be sort to higher QDC counts in the noise spectrum (see fig. 4.9(a)) than "normal" noise would be. The noise structure of the curve is continued over the expected range what ensures this theory.

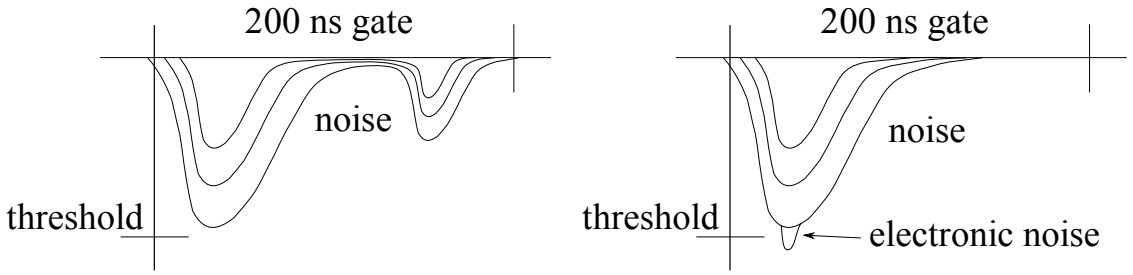

(a) Two or more noise signals together higher than the threshold.

(b) Noise signals and electronic noise together higher than the threshold.

Figure 4.9: Genesis of noise higher than the threshold.

The cyan curve (SiPM 1018 & SiPM 1019 & PMT) conforms the signal of vertical muons which is detected from every PM. The most probable value (MPV) in QDC counts should be the same for both SiPMs in a perfect arrangement.
SiPM 1019 has a MPV of about 1100 QDC counts and SiPM 1018 of about 1500 QDC counts. These MPVs reconfirm the assumption that SiPM 1018 is coupled better to the fibre than SiPM 1019.
The green curve (SiPM 1019) in (a) and (SiPM 1018) in (b) is expected to rise vertically to the first signal photon equivalent peak in theory, but the curve is flattened. One reason could be the photon noise together with electronic noise of the devices.
A normal noise could not top the threshold, but if a electronic noise is superimposed, the threshold is topped and lower QDC counts than the first photon equivalent are filled (see fig. 4.9(b)).

The most probable photon equivalent (MPPE) for signals of SiPM 1019 is 11 p.e. what corresponds to about 1100±50 QDC counts and for SiPM 1018 it is 10 p.e. that has about 1100±50 QDC counts.

4.2.1.2 Scintillator 6 mm

In the measurement with black felt with a thickness of 6 mm SiPM 1019 and SiPM 1018 have not such a big difference in their rates as in the measurement with a thickness of 8 mm. This confirmes that in the previous measurement the coupling of the SiPMs was different and now SiPM 1019 is coupled better than before. SiPM 1018 still has a higher rate that may is caused by the lower threshold.

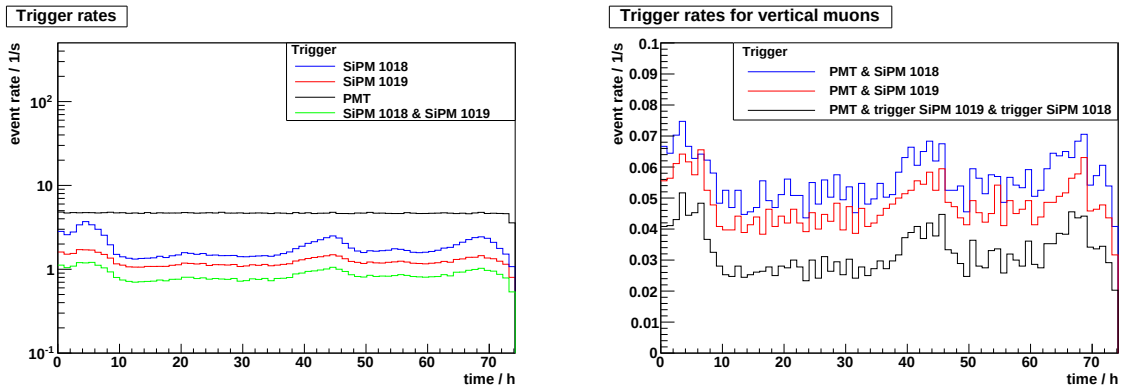

(a) Rates of single detectors with logarithmic ordinate

(b) Rates of vertical muons

Figure 4.10: Trigger rates of the measurement with black felt 6 mm.

Fig. 4.10 shows again the temperature dependency of the trigger rates.
The thinner scintillator (6 mm) has a volume of 75% of the scintillator with 8 mm thickness. Theoretically this would mean that the most probable photon equivalent of the thinner one is 75% of the thicker scintillator. SiPM 1019 has a MPPE of 11 p.e. what corresponds to about 1050±50 QDC counts and SiPM 1018 of 9 p.e. what is about 950±50 QDC counts. This is equal to ∼86% for SiPM 1018 and ∼95% for SiPM 1019 of the MPPEs from the thicker scintillator.
These discrepancy of theory and measurement could not be explained only with these measurements.

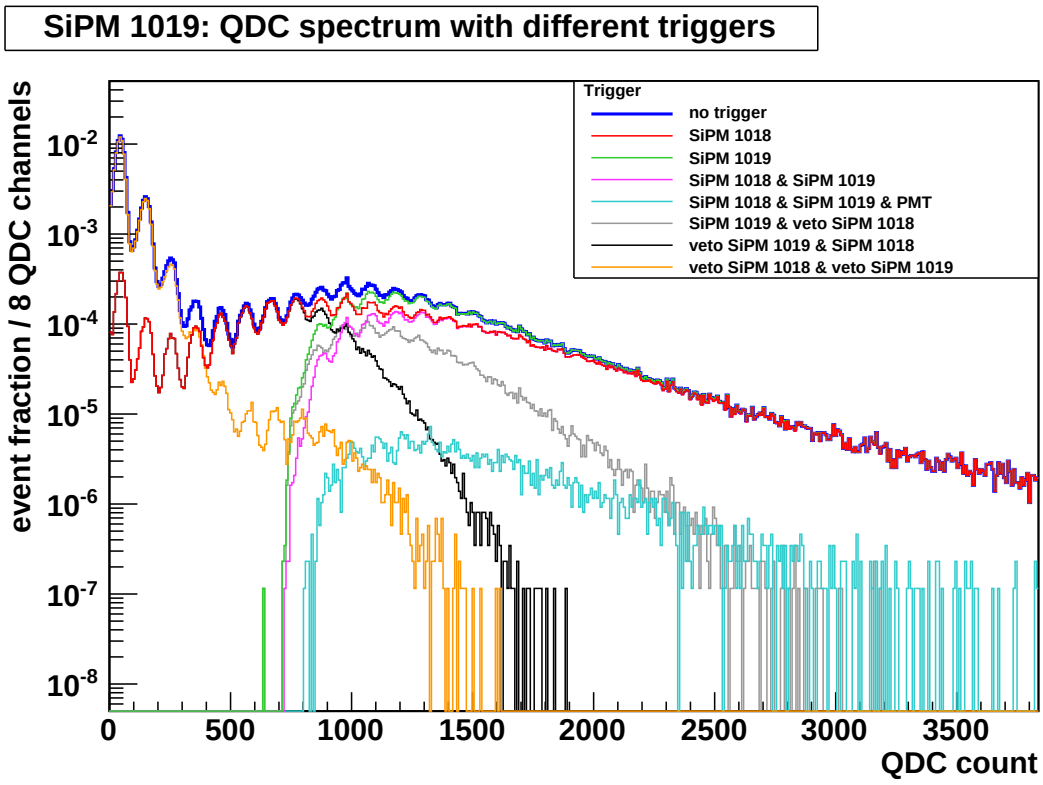

(a) QDC spectrum of channel 9

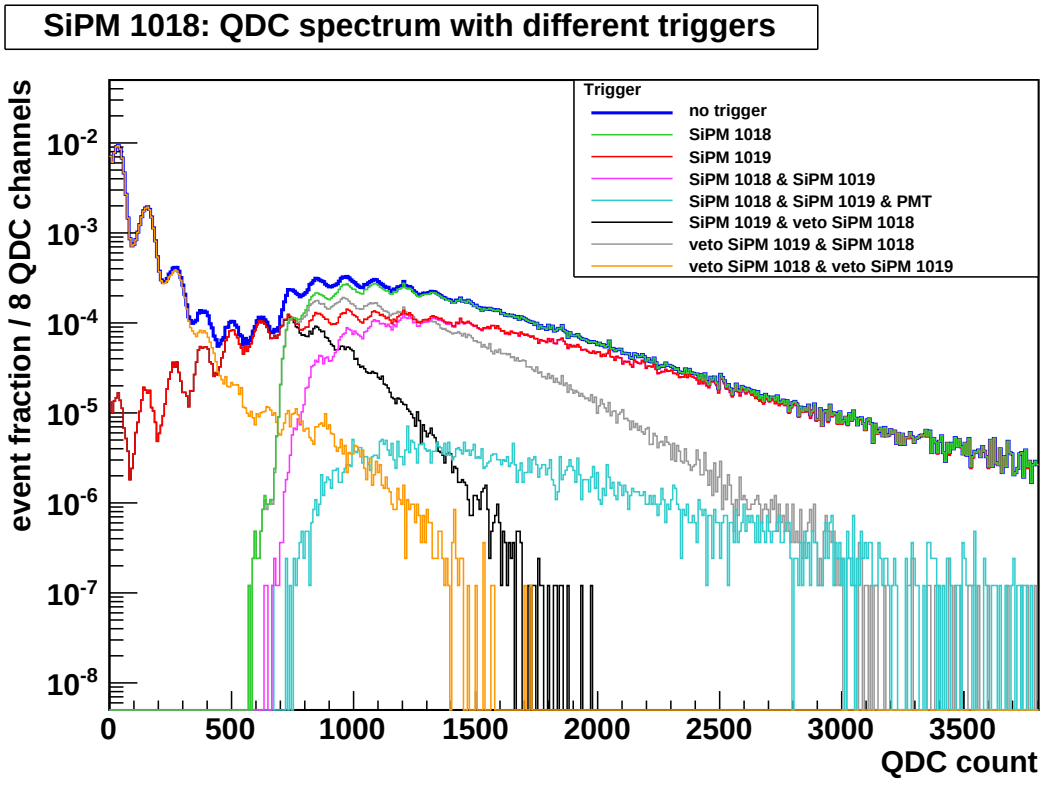

(b) QDC spectrum of channel 8

Figure 4.11: QDC spetra with different triggers of the measurement with black felt 6 mm.

Figure 4.11 shows the QDC spectra of both SiPMs with different triggers for the measurement with black felt and a thickness of 6 mm. The run of the curves are nearly the same as the ones of the measurement with a thickness of 8 mm.

4.2.2 TYVEK

4.2.2.1 Scintillator 8 mm

The trigger rates are much higher in the measurement with TYVEK as wrapping material than the rates in the measurement with black felt.
TYVEK rises the reflectivity and amplifies by that the photon efficiency, because the photons are reflected by the TYVEK into the scintillator again when they left the scintillator in contrast to black felt.
Again SiPM 1019 has a lower rate than SiPM 1018 (factor 5). As described before this is a reason of different threshold and coupling. Maybe the SiPM 1019 is a little bit crooked inside the metal box so that the wavelenght shifting fibre does not sit perfectly to the surface of the SiPM.

The rates for the single detectors fluctuate again with the temperature, but the rates for vertical muons are nearly constant. Here the single detector rates for the SiPMs are higher than the PMT rate and with that a constant rate for vertical muons is reached.

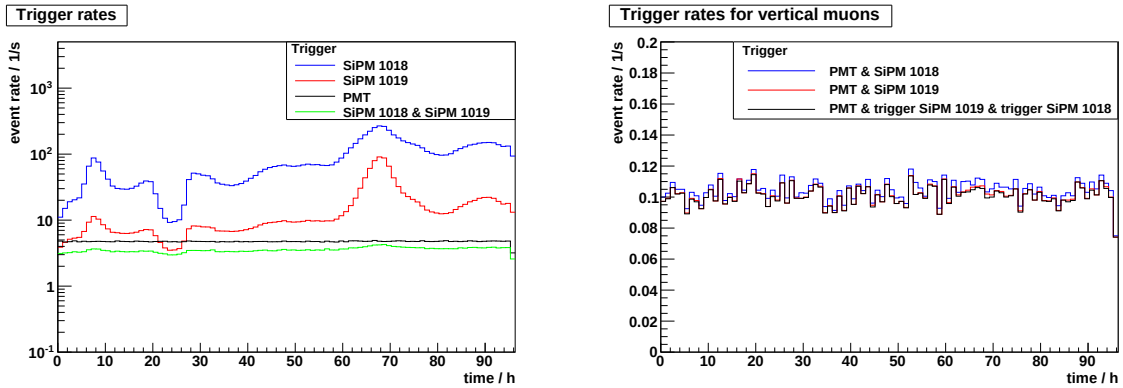

(a) Rates of single detectors with logarithmic ordinate

(b) Rates of vertical muons

Figure 4.12: Trigger rates of the measurement with TYVEK 8 mm.

In this measurement the most probable photon equivalent of SiPM 1019 is 7 p.e. what corresponds to 800±50 QDC counts and for SiPM 1018 it is 6 p.e. and 750±50 QDC counts. Here the orange curve (veto SiPM 1018 & veto SiPM 1019) has not such a “shoulder” (from 7 p.e. on) than the one in the measuerement with black felt. This is because the measuerement with black felt has a much higher temperature interval (3°C higher) and with that higher noise rates. But more noise means that the probability that two signals are in one gate rises.

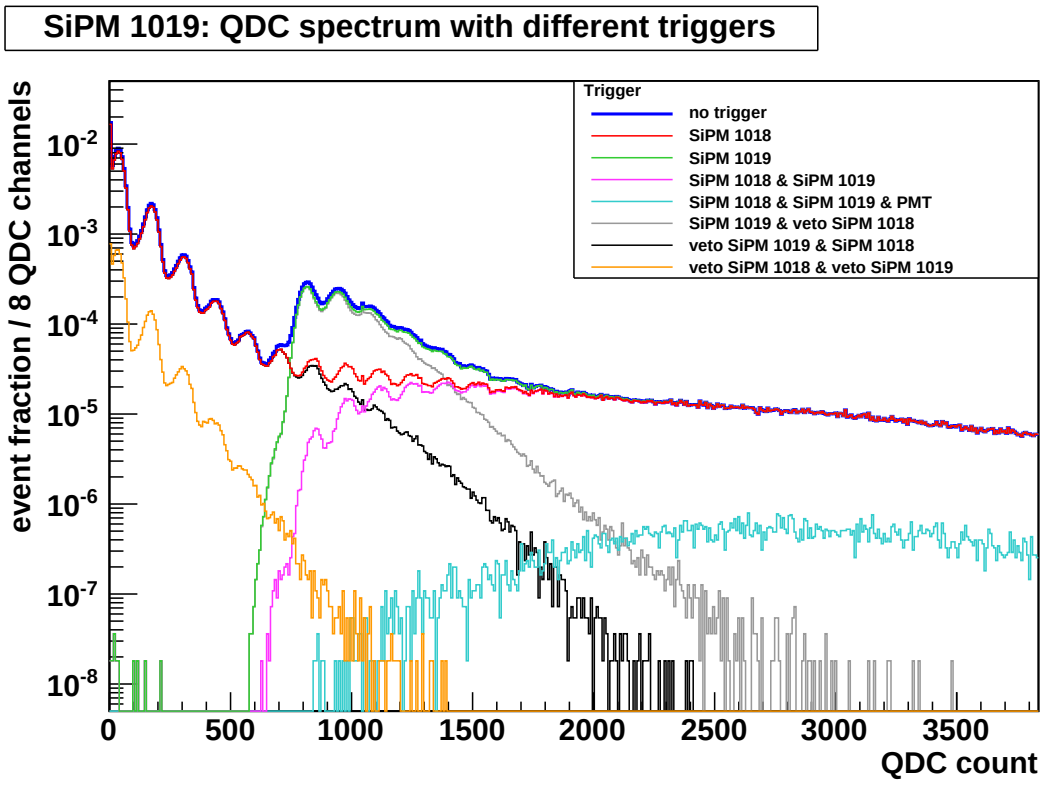

(a) QDC spectrum of channel 9

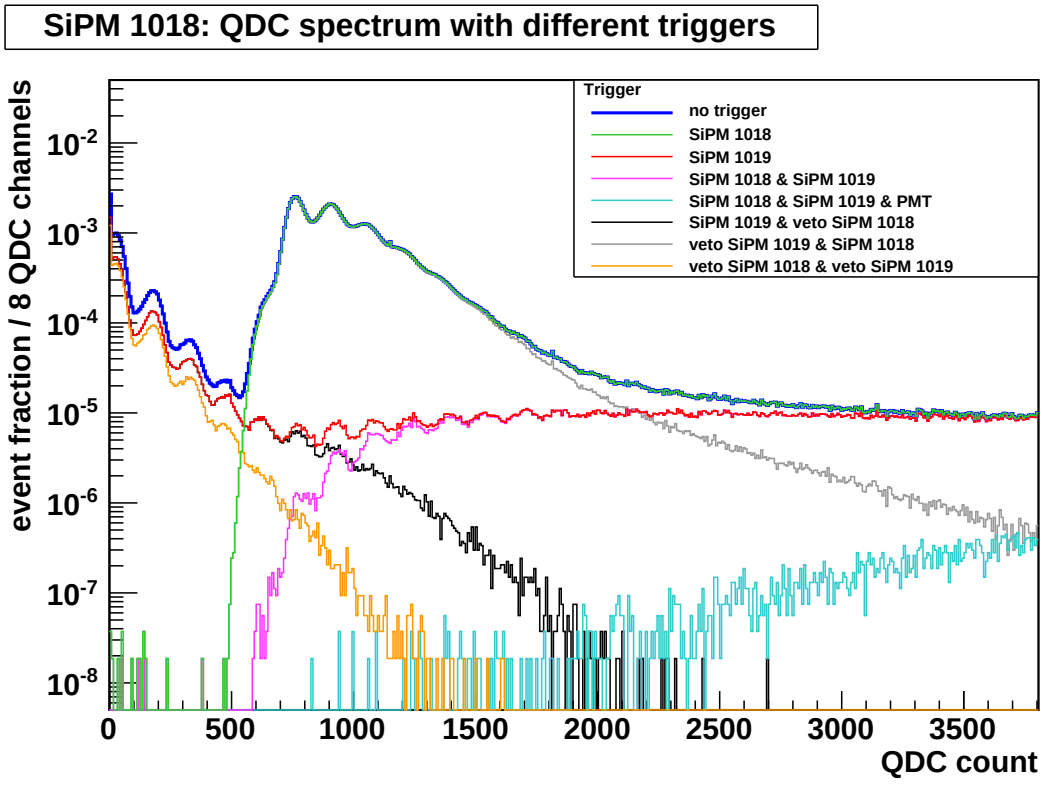

(b) QDC spectrum of channel 8

Figure 4.13: QDC spetra with different triggers of the measurement with TYVEK 8 mm.

4.2.2.2 Scintillator 6 mm

In the measurement with TYVEK and 6 mm thickness the trigger rates are a little bit higher that the ones for the thicker thickness. Normaly a lower rate was expected but the difference is very small and could be a reason of statistics.

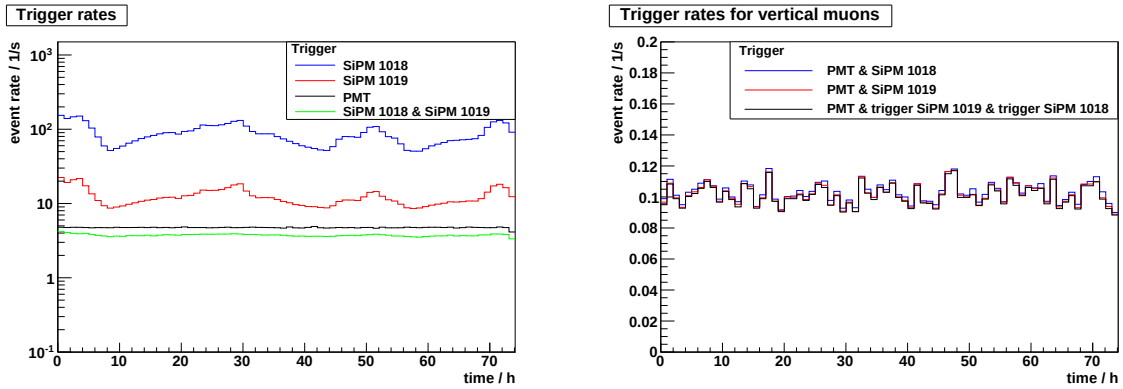

(a) Rates of single detectors with logarithmic ordinate

(b) Rates of vertical muons

Figure 4.14: Trigger rates of the measurement with TYVEK 6 mm.

Again all QDC spectra are normed to the blue curve (no trigger) and the value of the pedestal is determined by a gaussian fit and substrated to the data.

SiPM 1019 has a MPPE of 7 p.e. with 800±50 QDC counts and SiPM 1018 of 6 p.e. what corresponds to 750±50 QDC counts. This is the same as for the measurement with the thicker scintillator.
As said before it could not be explained with these few data. The QDC spectra seem to correspond more on the wrapping material than on the different thicknesses. Maybe the gain by using a wrapping material surmounts this effect.

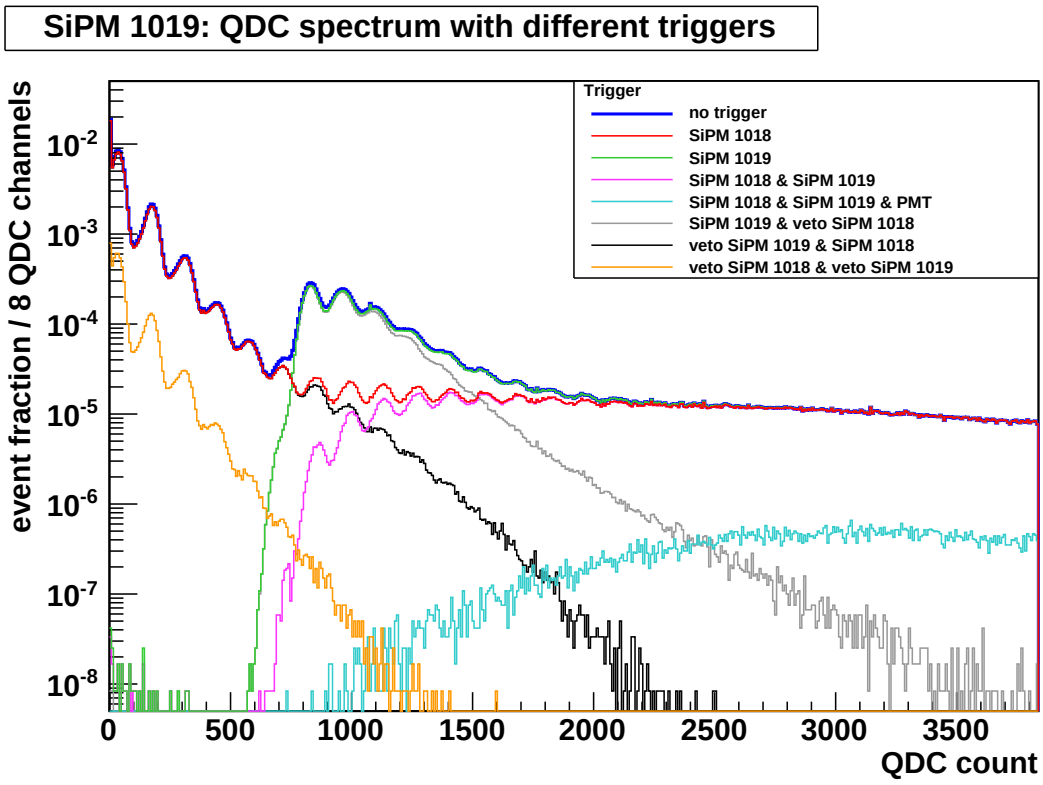

(a) QDC spectrum of channel 9

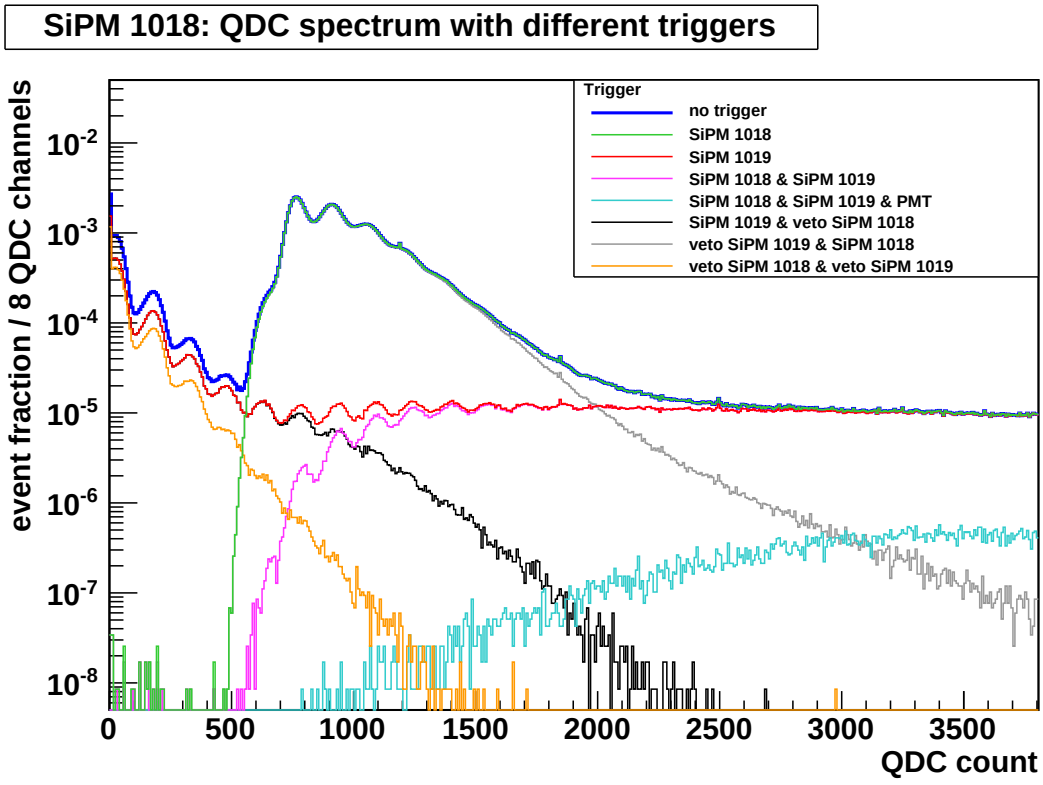

(b) QDC spectrum of channel 8

Figure 4.15: QDC spetra with different triggers of the measurement with TYVEK 6 mm.

4.2.3 Aluminium foil

4.2.3.1 Scintillator 8 mm

The aluminium foil is wrapped around the scintillator with the bright side inside. As described in chap.2.1.4 aluminium has a reflectivity of 88% [Han05] in comparison to TYVEK with a reflectivity of 90% [Gic98]. Thereof a lower photon rate for the measurement with aluminium foil is ecpected. The trigger rates confirm this expectation.
SiPM 1019 has a much lower rate than SiPM 1018 what supports the expectation of different coupling and threshold once again.

The expected correlation of temperature and event rate can be seen in fig. 4.16(a) again. This is the reason why the data are analysed at same temperature intervals (see also chap. 4.1.2).

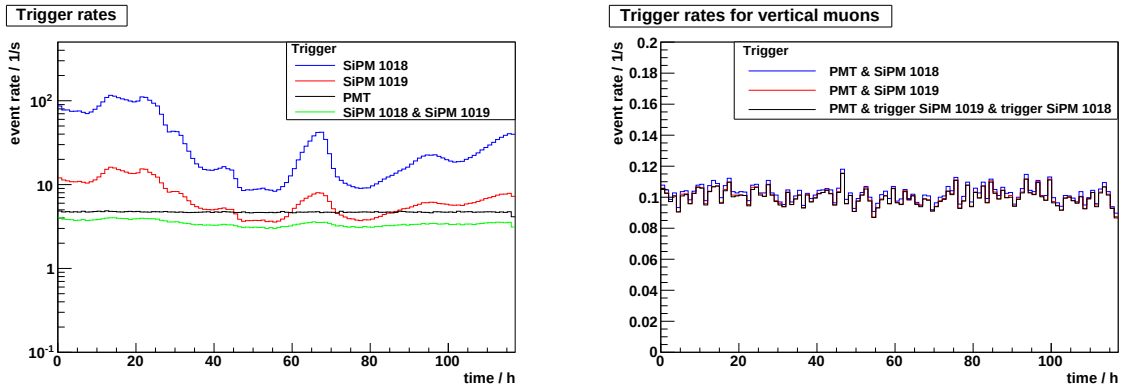

(a) Rates of single detectors with logarithmic ordinate

(b) Rates of vertical muons

Figure 4.16: Trigger rates of the measurement with aluminium foil 8 mm.

As described in the chapter of the measurements with black felt, the orange (veto SiPM 1018 & veto 1019) and green curve should not overlap. The reason why there is an overlap nevertheless is explained in this chapter, too. It is conspicuous that the orange curve in the measurements with reflector is not that high in the overlap range than in the measurements without reflector (black felt).
This could be a reason of the different temperature intervals. The measurement with black felt is at higher temperatures (26.6°C - 27.2°C) than the other ones (29.8°C - 30.3°C).
The noise is higher at higher temperatures and with that the probability that two noise signals are in one gate rises (see chap. 4.9). This could be a reason that the noise curve (orange) is higher in the measurement with black felt than the ones in the other measurements.

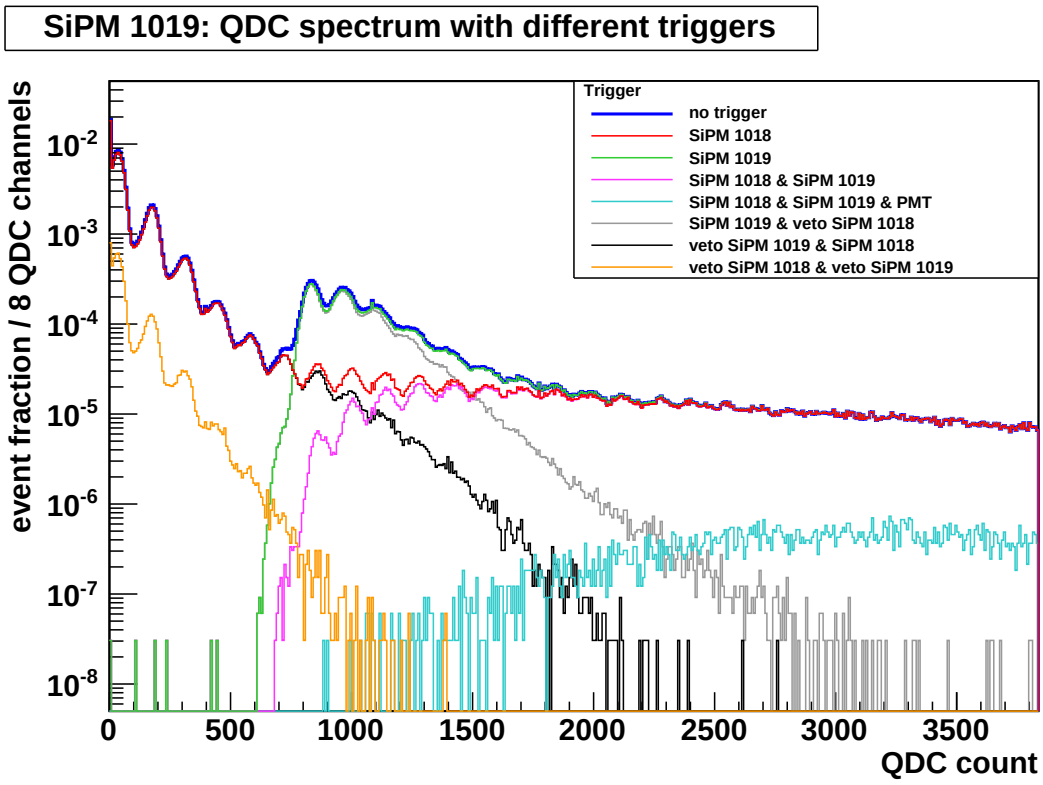

(a) QDC spectrum of channel 9

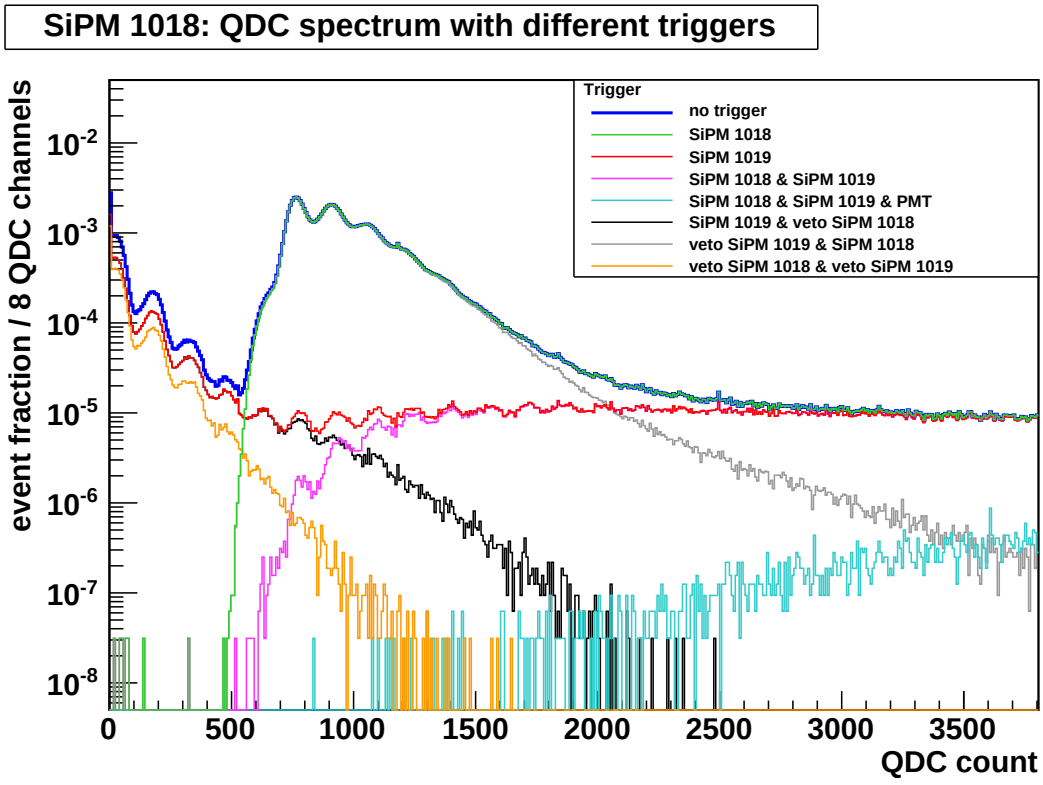

(b) QDC spectrum of channel 8

Figure 4.17: QDC spetra with different triggers of the measurement with aluminium foil 8 mm.

In the measurement with aluminium foil the most probable photon equivalent for SiPM 1019 is 7 p.e. with 800±50 QDC counts and for SiPM 1018 it is 6 p.e. what corresponds to 750±50 QDC counts. TYVEK and aluminium foil are both good reflectors and have not very significant differences, what can be seen among other things in their MPPEs which are the same.

4.2.3.2 Scintillator 6 mm

The results of the measuerements with aluminium foil and a thickness of 6 mm are equal to the other measuerements with a reflective wrapping material. As expected aluminium foil has little lower rates than the ones with TYVEK and there is not a significant difference to the measurement of aluminium foil with a thickness of 8 mm.

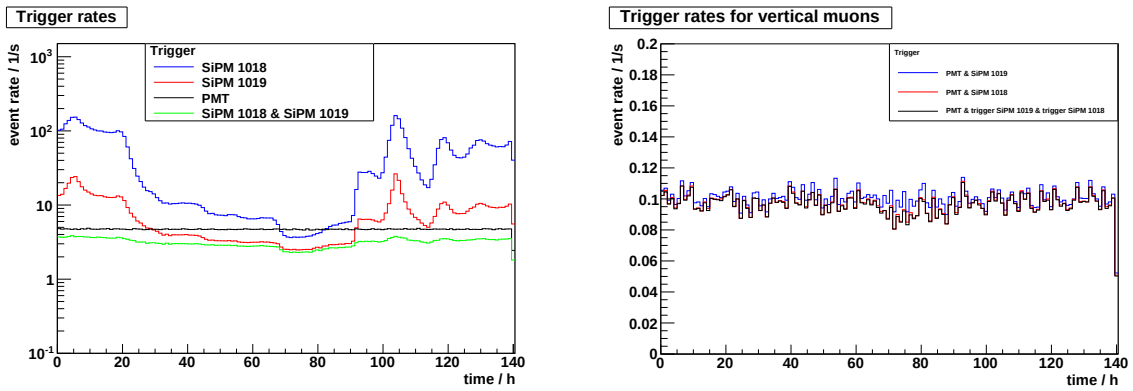

(a) Rates of single detectors with logarithmic ordinate

(b) Rates of vertical muons

Figure 4.18: Trigger rates of the measurement with aluminium foil 6 mm.

Here the MPPEs are the same as for the measurement with the thicker scintillator wrapped in aluminium foil. SiPM 1019 has a MPPE of 7 p.e. what corresponds to 800±50 QDC counts and SiPM 1018 of 6 p.e. with 750±50 QDC counts.

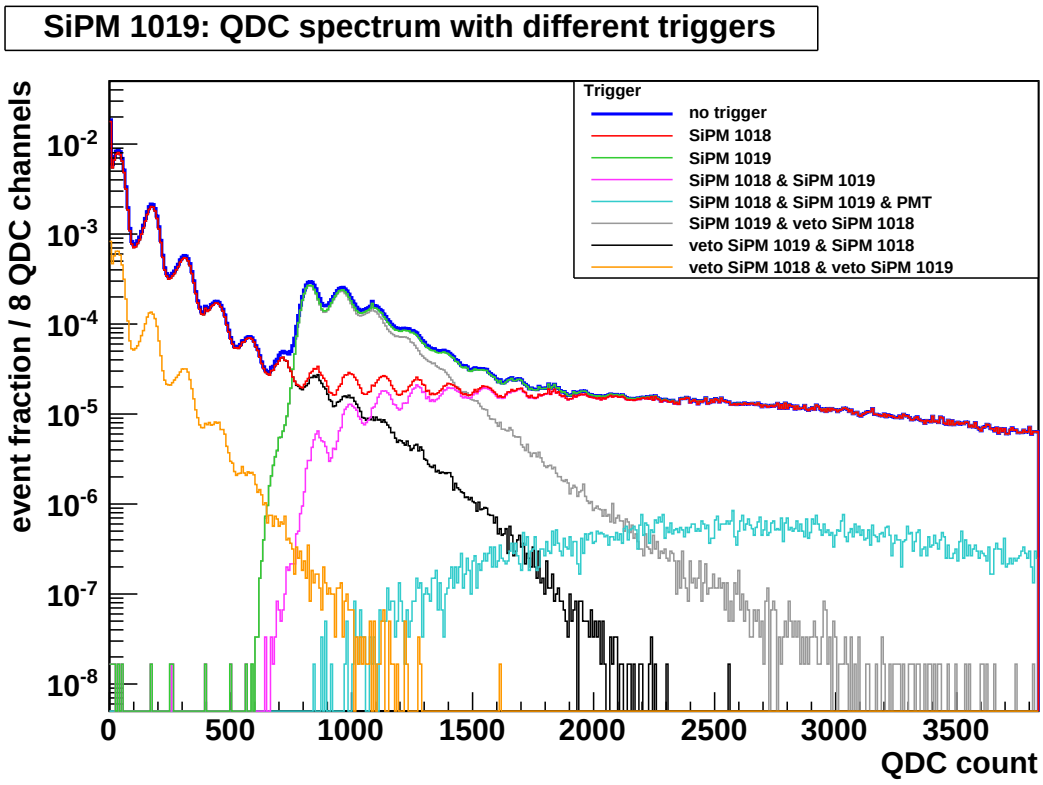

(a) QDC spectrum of channel 9

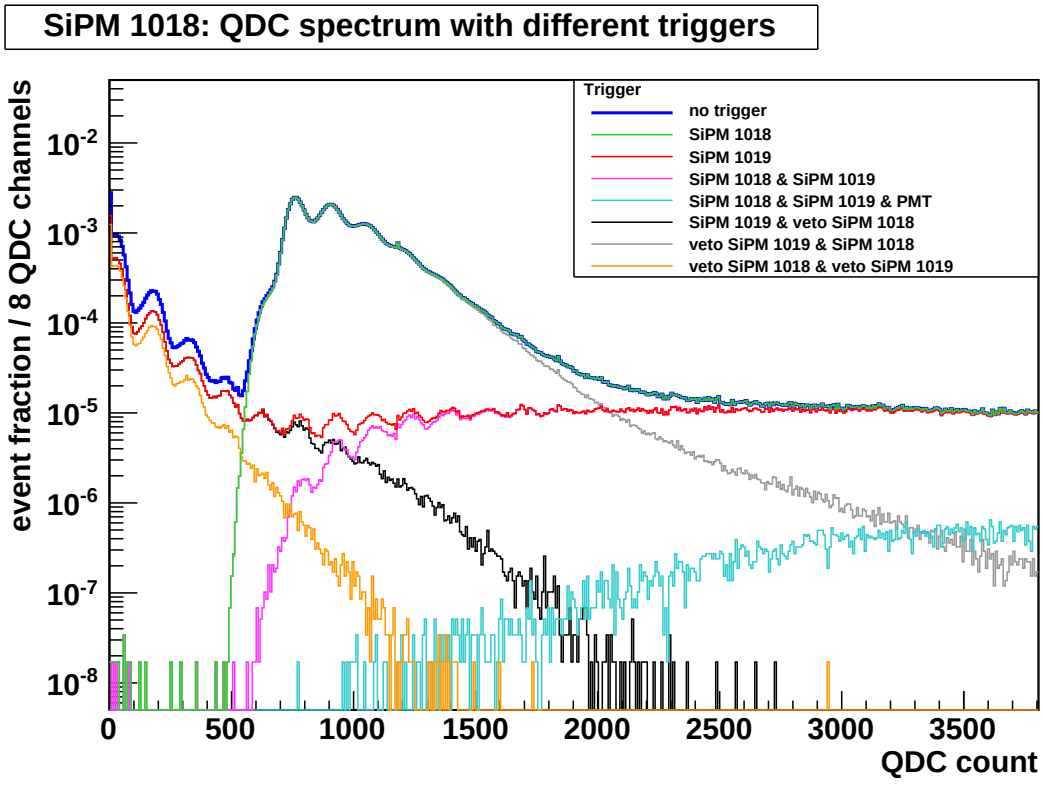

(b) QDC spectrum of channel 8

Figure 4.19: QDC spetra with different triggers of the measurement with aluminium foil 6 mm.

4.3 Summary of the measurements

The rate of the PMT shows no temperature dependency and has a constant rate of 4.7 s^{-1} (see tab. 6).
The measurement with TYVEk has the highest rates but there is no significant difference between the two scintillator thicknesses. The low variation is a result of statistics. The wrapping materials raise the rates for vertical muons with a factor of ∼3 in comparison to no reflector simulated with black felt.

Table 6: Total trigger rates of the measurements in s^{-1}

Trigger	felt 8 mm	felt 6 mm	TYVEK 8 mm	TYVEK 6 mm	Al 8 mm	Al 6 mm
SiPM 1019	1.0	1.3	15.3	12.3	7.2	7.3
SiPM 1018	3.0	1.8	84.4	86.6	36.5	41.0
SiPM 1019 & SiPM 1018	0.9	0.9	3.6	3.8	3.5	3.1
PMT	4.7	4.7	4.7	4.7	4.7	4.7
PMT & SiPM 1019 & SiPM 1018	0.04	0.03	0.10	0.10	0.10	0.10

The thickness of the scintillators has no detectable influence on the most probable photon equivalent in this setup (see tab. 7). Heaving regard to the limited space in the MTT in CMS at CERN where such a detector may be installed a thinner one would be more practically.
The measurement with black felt was at temperatures about 3°C higher than the other ones. The higher QDC counts of the most probable photon equivalent could be explained with the resulting higher noise rate in this measurement. As described in 4.9 the probability that two signals are in the same gate rises with more noise and thereby higher QDC counts are filled.

Table 7: Most probable photon equivalents of the measurements in QDC counts

SiPM	felt 8 mm	felt 6 mm	TYVEK 8 mm	TYVEK 6 mm	alu 8 mm	alu 6 mm
1019	11 p.e. 1100±50	11 p.e. 1050±50	7 p.e. 800±50	7 p.e. 800±50	7 p.e. 800±50	7 p.e. 800±50
1018	10 p.e. 1100±50	9 p.e. 950±50	6 p.e. 750±50	6 p.e. 750±50	6 p.e. 750±50	6 p.e. 750±50

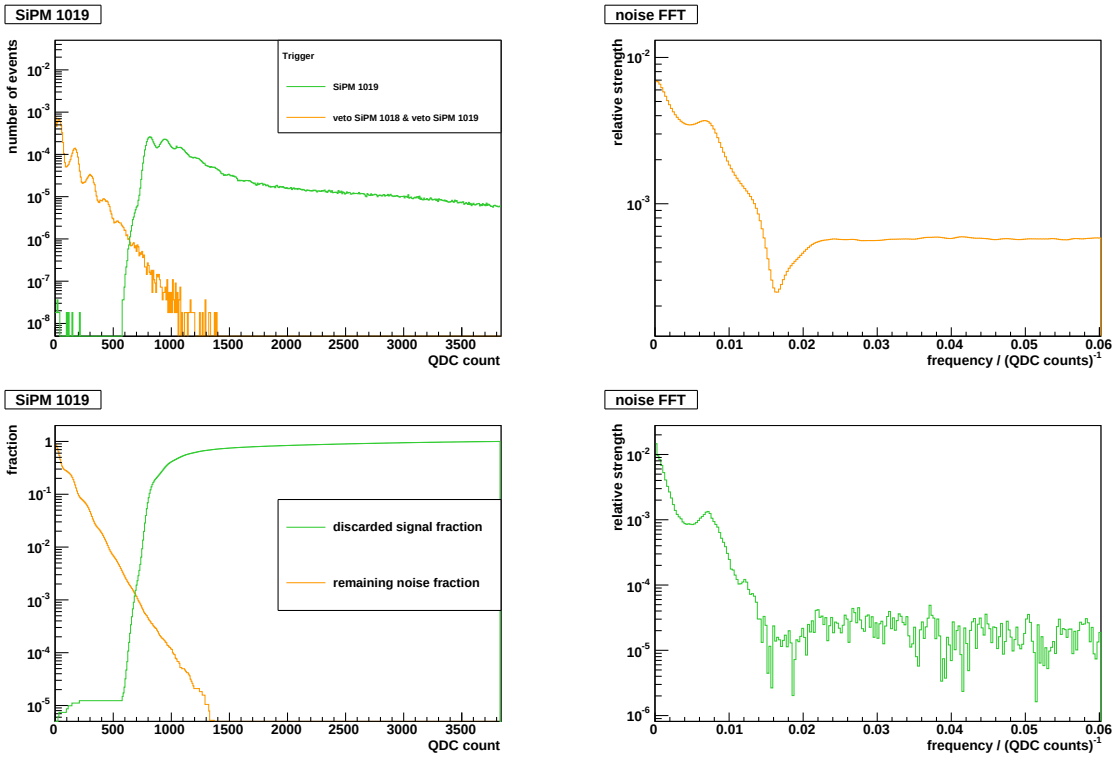

(a) Noise and signal fraction with logarithmic ordinate.

(b) Fourierspectra of noise and signal with logarithmic ordinate.

Figure 4.20: Measuerment with TYVEK and a thickness of 8 mm.

Figure 4.20(a) shows exemplarly for TYVEK 8 mm the noise (orange curve) and the signal (green curve) in the upper plot and their fraction in the lower plot.
A cut on the QDC counts at about 600 QDC counts seperates signal from noise with $\sim$0.05% noise left.
In fig. 4.20(b) the fourierspectra of noise and signal are shown. The period lenght is the inverse of the frequency.
The noise spectra has a period lenght of about 154$\pm$1 QDC counts what corresponds to the distance between two p.e. peaks in the orange noise curve. The photon equivalents of the signal have a distance of about 142$\pm$1 QDC counts (see tab. 8).

Again the results for the measuerement with the thinner scintillator have no significant difference to the ones with the thicker scintillator.

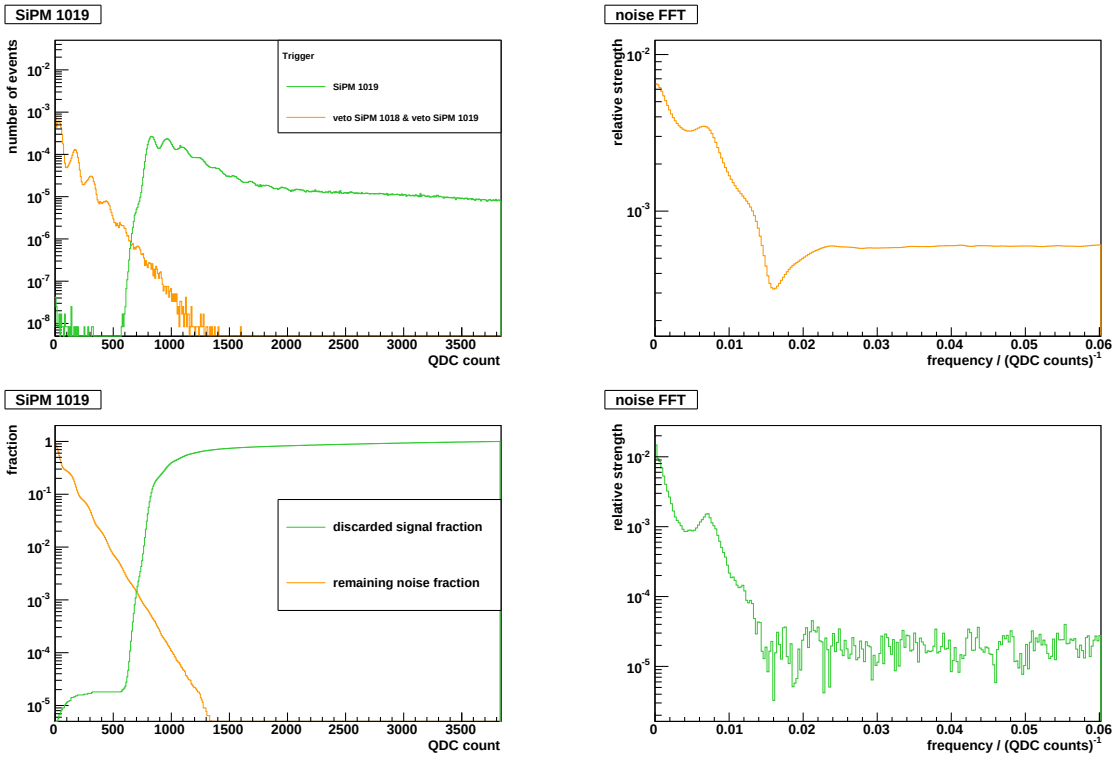

(a) Noise and signal fraction.

(b) Fourierspectra of noise and signal.

Figure 4.21: Measuerment with TYVEK and a thickness of 6 mm.

Table 8: FFT period length / (QDC counts) of the measuerements with SiPM 1019

	felt	TYVEK	Al
8 mm			
noise	120±1	154±1	154±1
signal	106±1	142±1	147±1
6 mm			
noise	120±1	154±1	154±1
signal	106±1	142±1	142±1

The period lenght of the signal from SiPM 1019 with black felt is about 106±1 QDC counts and with TYVEK about 142±1 QDC counts. With that a gain of about 75% with TYVEK 8 mm and about 72% with aluminium foil could me calculated.
The different threshold of SiPM 1018 has an influence on the period lenght (tab. 9) and with that on the gain of the signal of about 77%.

Table 9: FFT period length / (QDC counts) of the measuerements with SiPM 1018

	felt	TYVEK	Al
8 mm			
noise	141±1	172±1	182±1
signal	123±1	159±1	159±1
6 mm			
noise	141±1	180±1	182±1
signal	123±1	159±1	159±1

5 Conclusion and outlook

5.1 Setup

It would be easier to handle the setup if the WLS fibre would not be longer than the scintillator, because that is very sensitive towards breaking. It has just 1 mm in diameter but the fibre is about 1 cm longer than the scintillator.
This sticked out part is wrapped with a plastic cylinder and need to install in the metal box where the SiPM is. This is a very delicately zone of the setup.
In future an other setup would be more effective. Such a setup need to handel different scintillator dimensions and with that other wrapping materials and their different thicknesses, too.
To realise that the amplifier boards with the SiPMs need to be more movable and not be stopped at a fixed point.

5.2 Temperature

As described in chap. 4.1.2 the results of measurement are correlated to the actual ambient temperature. This causes problems while comparing the different measurements with other wrapping materials and during the comparison between the two different scintillator thicknesses. To round this problem an air conditioner in the experimental rooms would help so that the temperature is constant during the whole measurement.

5.3 Measurement of cosmic muons

Though some problems appeared during the measurement the photon equivalent peaks could be seperated well, the expectations were fullfilled and a good reflector was found. TYVEK has a similar efficiency as aluminium foil, but the foil cracks easily espacially at the corners and where the waveleght shifting fibre leaves the scintillator. This is a pro for using TYVEK as wrapping material. Moreover TYVEK is inexpensive, waterproof and hard crackable.
The setup and the used devices work well together. A controlling of temperature would be detter as described before, but a measurement over 5 - 6 days collects enough statistics to limit the evaluation range to same temperatures.
From this it follows that the prototype detector that is characterised in this thesis could measures cosmic muons, well.

In future the setup could be upgraded with a temperature control and easier possibilities to switch different scintillators. Other scintillator thicknesses could be characterised to proofe the dependency of the trigger rate more detailed. Thereof other dimensions than 10×10 cm^2 and different waveleght shifting fibres could be used, e.g. thicker fibres, cornered fibres and fibres that do not run straight through the scintillator.
The gate width of 200 ns coud be systematically reduced to ensure that only one signal is in the gate. The treshold need to be adjusted more precisely and a with smaler temperature interval the photon equivalent peaks would be clearer seperated.

References

[Bar04] Joelle Barral. Study of silicon photomultipliers. *Diplomarbeit*, 2004.

[CAE08] CAEN. Technical information manual mod. v965/v965a. 2008.

[CI05] Saint-Gobain Ceramics and Plastics Inc. Premium plastic scintillators. 2005.

[Din06] N. Dinu. Development of the first prototypes of silicon photomultiplier at itc-irst, 2006.

[EHG01] K. Bressler E. Hering and J. Gutekunst. Elektronik fur ingenieure. 2001.

[Gic98] Justus Ogwoka Gichaba. Measurements of tyvek reflective properties for the pierre auger project. *Diplomarbeit*, 1998.

[GS07] T.K. Gaisser and T. Stanev. Cosmic rays. 2007.

[Han05] Joseph F. Hanlon. Handbook of package engineering. Technical report, 2005.

[Heb10] Prof. T. Hebbeker. *private communication*, 2010.

[K.K10] HAMAMATSU PHOTONICS K.K. Mppc: Multi-pixel photon counter, 2010.

[Mer10] M. Merschmeyer. *private communication*, 2010.

[Pap10] P. Papacz. Optimisation of the particle detection efficiency for scintillation detectors with sipm readout. diplomarbeit, 2010.

[Pro08] Maxim Integrated Products. Ds18b20 programmable resolution 1-wire digital thermometer, 2008.

[Ren10] J. Rennefeld. Studien zur eignung von silizium photomultipliern fur den einsatz im erweiterten cms detektor am slhc. *Diplomarbeit*, 2010.

[RL09] D. Renkera and E. Lorenz. Advances in solid state photon detectors. 2009.

[SG05] Saint-Gobain. Ceramics and plastics inc. scintillation products, scintillating optical fibres. 2005.

[Tec07] Eljen Technology. Ej-500 optical cement. 2007.

[Wik07] The Free Encyclopedia Wikipedia. `http://en.wikipedia.org/wiki/File:Atmospheric_Collision.svg`. 2007.

Appendix

Noise

Table 10: Noise data of the SiPMs (to fig. 4.2)

	threshold / photons	noise rate / kHz
1018 SiPM		
	0.5	726.000 ± 28.000
	1.5	180.000 ± 8.000
	2.5	33.000 ± 5.000
	3.5	5.800 ± 1.150
	4.5	0.997 ± 0.341
	5.5	0.221 ± 0.103
	6.5	0.027 ± 0.025
1019 SiPM		
	0.5	733.000 ± 12.500
	1.5	151.000 ± 3.500
	2.5	27.000 ± 2.000
	3.5	4.500 ± 0.600
	4.5	0.763 ± 0.177
	5.5	0.133 ± 0.089
	6.5	0.022 ± 0.015

List of Figures